Diapycnal Mixing Transience and the Meridional Overturning Circulation

by

William R. Boos

B.S. Physics, B.A. Mathematics
State University of New York at Binghamton, 1997

Submitted to the Department of Earth, Atmospheric and Planetary Sciences
in partial fulfillment of the requirements for the degree of

Master of Science in Geosystems

at the

MASSACHUSETTS INSTITUTE OF TECHNOLOGY

June 2002

Author .....
Department of Earth, Atmospheric, and Planetary Sciences
May 7, 2002

Certified by .....
Kerry Emanuel
Professor
Thesis Supervisor

Accepted by.....
Ronald Prinn
Head, Department of Earth, Atmospheric and Planetary Sciences

Diapycnal Mixing Transience and the Meridional Overturning Circulation

by

William R. Boos

Submitted to the Department of Earth, Atmospheric and Planetary Sciences
in partial fulfillment of the requirements for the degree of
Master of Science in Geosystems

Abstract

Diapycnal mixing of ocean waters is crucial to the dynamics and associated heat transport of the meridional overturning circulation, yet uncertainty exists regarding the distribution and physical mechanisms of this mixing. This study uses a highly-idealized, single-hemisphere model of buoyancy-forced flow to examine the examine the effects of the transience of diapycnal mixing on the MOC. The strength of the MOC was found to be insensitive to mixing transience when mixing occurred uniformly on basin boundaries. For mixing that was highly localized in space, a ten-fold increase in transience, as compared with the time-invariant control, resulted in a decrease by about 20% of MOC mass and heat transport. The degree of sensitivity in the highly localized case is likely to be a strong function of the surface restoring timescale for temperature. The circulation dynamics associated with transient mixing displayed large-scale, complex oscillations that increased in amplitude with the transience of mixing. Attempts to quantify the relationship between mixing transience, MOC strength, and the power expended in mixing were inconclusive and merit further investigation.

Thesis Supervisor: Kerry Emanuel
Title: Professor

Table of Contents

List of Figures

List of Tables

Chapter 1

Introduction

1.1 Motivation

The transport of heat from equatorial regions toward the poles is crucial to regulation of the earth's climate and to the dynamics of climate change. The oceans carry about one-half to one-third of the total meridional heat flux, as estimated by subtracting the measured atmospheric meridional flux from the total flux required for the net radiative balance at the top of the atmosphere [Hartmann, 1994; Macdonald and Wunsch, 1996]. The deep meridional overturning circulation (MOC) is thought to be a determining factor in climate because it carries a large part of the oceanic meridional heat flux [Hall and Bryden, 1982].

Although the MOC transports a large amount of heat, estimated at 2×10^{15} W, it is not driven by heat in that density changes due to the surface heat flux are spatially distributed so as to result in a change in the potential energy of the ocean that is too small to drive the overturning [Munk and Wunsch, 1998, Faller, 1968, Oort et al, 1994]. Sandstrom (1908) showed that a basin of fluid heated from above would equilibrate into a stratified, stable state with some small, near-surface convective motion. Jeffreys (1925) extended this result by showing that it held only in the absence of mixing that carried warm, less dense fluid across surfaces of constant density to a lower potential.

The numerous processes of diapycnal (non-convective) mixing are often represented as a balance between advection and diffusion of the form

$$w\frac{\partial \rho}{\partial z} = \kappa_h \frac{\partial^2 \rho}{\partial z^2} \qquad (1)$$

where w is the upwelling velocity, ρ is the fluid density, and κ serves as a parameterization of the strength of diapycnal mixing. Measurements have shown that away from topography and basin boundaries, this diffusivity has the pelagic value $\kappa_{PE}=10^{-5}$ m^2/s [Osborn and Cox, 1972]. Near some boundaries, diffusivities up to 10^{-1} m^2/s have been measured [Polzin et al., 1995, 1997].

Uncertainty exists regarding the distribution of mixing in the oceans and the exact physical mechanisms by which it is produced. Using ocean general circulation models (OGCMs) to simulate how the MOC might be affected by variations in mixing could aid in understanding the causes of mixing and provide clues as to where to look for enhanced mixing when taking *in situ* measurements. Such simulations might also provide information on how climate could be affected by changes in the energy expended in mixing or in the distribution of mixing. Scott and Marotzke (2001) used an idealized OGCM to examine how changes in the spatial distribution of diapycnal mixing affected the MOC, and briefly reviewed other studies which have used models to explore the effect of mixing location on ocean circulation. Little consideration has been given to the temporal distribution of mixing.

Emanuel (2001) proposed tropical cyclones as a mechanism for producing mixing that drives the MOC. Tropical cyclones are known to be efficient mixers of the upper ocean, mixing the warm waters of the isothermal mixed layer across isopycnals into the colder waters of the thermocline. This results in a temporary deepening and cooling of the mixed layer, and a temporary warming of the upper thermocline. Over several months, the negative temperature anomaly in the mixed layer is removed by a downward heat flux through the ocean surface. This amounts to a positive net heating of the water column under the track of the tropical cyclone. Emanuel estimated the net vertical heating produced by global tropical cyclone activity to be $(1.4 \pm 0.7) \times 10^{15}$ W. If this net vertical heating were balanced by an average meridional heat flux out of the tropics, then it could account for a significant part of the 2×10^{15} W of estimated ocean meridional heat flux.

Emanuel's theory provides additional motivation for studying the effect of transience in diapycnal mixing on the meridional overturning circulation, because mixing induced by tropical cyclones would occur on much shorter timescales than that produced by tides. It also raises the question of whether feedback processes involving ocean mixing exist between climate state and meridional heat transport.

1.2 Previous Work

Scott and Marotzke (2001) employed an ocean circulation model to explore the effect of the location of diapycnal mixing on the MOC. Using an idealized three-dimensional model of buoyancy-forced flow in a single-hemisphere basin, they found the strength of the MOC and its associated heat transfer to be determined mainly by low-latitude mixing in the thermocline. Mixing at ocean boundaries was found be more efficient than interior mixing at driving the MOC.

Scott and Marotzke also explored the effect of mixing location on upwelling profiles, boundary flows, and abyssal stratification. They found that abyssal mixing does not contribute significantly to the MOC, and suggested that enhanced boundary mixing in the thermocline should be identified in observations.

1.3 Thesis Description

This study expanded on the modeling of the MOC performed by Scott and Marotzke (2001), who considered mixing as a function of three spatial coordinates only. The same numeric model was used, with minor changes in parameters and methodology, to explore the sensitivity of the MOC to the temporal distribution of mixing. The functional form of the dependence of mixing on time was kept to a simple step function with a timescale on the order of months and a period of one year, so that for a given spatial distribution of mixing, the diapycnal diffusivity was toggled between some maximum value and the minimum pelagic value.

Consideration was given to conserving the total work done by mixing between different model runs, because it is expected that the total energy available for mixing will be constant in a given climate regime. This issue is discussed in detail below, given that it was not trivial to either set or calculate the total energy expended in mixing.

The methods used in this study were not intended to simulate naturally occurring mixing processes, but instead to serve as an idealized, large-scale parameterization of buoyancy diffusion. Examining the effect that transience in this parameterization has on the MOC may provide insight into the physical processes that actually mix the oceans.

Chapter 2

Methods

2.1 Description of the Model

This study used the Modular Ocean Model (MOM) developed by the Geophysical Fluid Dynamics Laboratory (GFDL/NOAA Department of Commerce) to simulate circulation in a single-hemisphere ocean basin. Scott and Marotzke used version 2.0 of MOM 2 for their runs, and even though a later release was available at the time of this study, MOM 2 version 2.0 was used again to facilitate direct comparison with the runs of Scott and Marotzke.

MOM uses finite difference methods to numerically solve the primitive equations of ocean circulation: the Navier-Stokes equations and a nonlinear equation of state that relates temperature and salinity to fluid velocity. The Boussinesq, hydrostatic, and rigid lid approximations are used in solving the Navier-Stokes equations [MOM 2 Documentation User's Guide and Reference Manual].

Diapycnal mixing is implemented in MOM through the vertical diffusion of buoyancy. This is a reasonable approximation because isopycnal surfaces are close to horizontal over much of the ocean, especially at the low latitudes where mixing was applied in this study. This parameterization made it possible to control the magnitude of simulated diapycnal mixing by setting the value of the vertical diffusivity coefficient κ. In this study a minimum value of 10^{-5} m^2/s was used for κ to simulate the pelagic diffusivity, and κ was set to higher values in grid cells where mixing was applied.

The spatial domain was set to a single hemisphere basin 60° in longitude by 64° in latitude, with the southern boundary at the equator, the western boundary at 0° longitude, and a constant depth of 4500 meters. Table 1 lists these and other significant model parameters. No topography was included and the only atmospheric coupling was through application of a simple, time-invariant wind stress that varied with latitude only. This idealized wind stress fit a cosine profile and consisted approximately of easterlies across the southern half of the domain and westerlies across the northern half. The model was forced by zonally constant surface boundary conditions for temperature and salinity,

which fit an identical cosine profile with a maximum at the equator and respective peak-to-peak amplitudes of 27° C and 1.5 psu. Temperature and salinity had identical restoring time constants of 30 days.

The model was run at a resolution of 3.75° zonally x 4° meridionally x 16 levels vertically. Although Scott and Marotzke performed most of their runs at the higher resolution of 1.875° x 2° x 30 vertical levels, they noted that results did not differ significantly when the lower resolution was used. This study used the lower resolution to reduce computation time. A larger time step was also used with similar reasoning: 24 hours for tracers and 1 hour for velocity and density.

2.2 Experiments and Parameters

After initial experimentation with various mixing regimes and methods of time variation, two categories of runs conducted by Scott and Marotzke were selected as the basis for this study. The first category consisted of runs where mixing was applied in all grid cells adjacent to a basin boundary, and the second consisted of runs where mixing was applied entirely in one grid column away from boundaries in the subtropics, centered at 10° N and 24.375° E (table 2).

For each category, a set of runs was performed where mixing was applied for 12 months (the control case), 6 months, 3 months, 2 months, and 1 month of each year. The months in which mixing was applied were contiguous within each year, and κ was changed as a step function of time between the "off" value of 0.1 cm^2/s and the "on" value used for each particular run (table 3), with no variation in the vertical. The boundary mixing run with no time variation (12 months/year of mixing) was made identical to that of Scott and Marotzke by using the same value of κ in boundary cells. The time-weighted diffusivity of each boundary mixing run was held the same as this control run. For runs with highly localized mixing, the diffusivities were set so that the area-weighted diffusivity was equal to that of latitudes from 0° to 36° N for the corresponding boundary mixing run. This was done because Scott and Marotzke found that boundary mixing at latitudes greater than 36° N did not contribute to the strength of the MOC. Thus, in all runs performed for this study, the area- and time-weighted diffusivity for latitudes 0° - 36° N was constant.

Integration for each run was started from the same equilibrium state and conducted until an annual mean equilibrium was again achieved, as indicated by zero annual mean heat exchange with the atmosphere and a constant annual mean meridional overturning. Annual means were used as equilibrium indicators because the model was forced by diffusivities that varied with time over the course of each year but had invariant annual means. Test runs indicated that about 200 years of simulation time were needed to reach the new equilibrium state.

2.3 Diagnostics

MOM contains a suite of diagnostic routines that output the state of model variables at desired intervals. The equilibrium values of the maximum meridional overturning and the net northward oceanic heat flux are the key variables for this study; diagnosing these quantities every five days over the course of one year at equilibrium was found to be sufficient for capturing the dynamics. Before the equilibrium state was reached, the maximum overturning and the basin-averaged ocean-atmosphere heat flux were measured five times each year.

Once annual mean equilibrium was reached, the detailed state of the circulation was diagnosed by taking instantaneous values of the velocity, density, and tracer fields once every five days for one year at equilibrium. These snapshots were used to create cross sections of the overturning streamfunction as well as the velocity and temperature fields. Much of this methodology was taken from Scott and Marotzke.

2.4 Calculation of Mixing Power

Ideally, we would like to hold constant the total energy expended in mixing as the transience of mixing varied. However, mixing power in MOM can not be set a priori, and so the time- and area-weighted diffusivity for low latitudes was held constant, as discussed above, and the spatially-integrated, annual-mean mixing power was calculated for each run.

The rate of work per unit mass done by diapycnal mixing in a stratified fluid is represented by ε and given by

$$\varepsilon = \kappa \frac{g}{\rho}\left(-\frac{d\rho^*}{dz}\right) \tag{2}$$

where ρ^* is the potential density of the fluid, and g the acceleration of gravity. This quantity is integrated vertically to obtain an expression for the power P expended by diapycnal mixing:

$$P = \int_0^h \rho \varepsilon dz = -\int_0^h g\kappa \frac{d\rho^*}{dz} dz \tag{3}$$

In this model, κ is a function of horizontal position and time only. Two methods were used to estimate this quantity for each run. The first assumed that potential density was a linear function of potential temperature, i.e. that the model used a linear equation of state. While MOM employs a nonlinear equation of state, this may nevertheless serve as a useful first order approximation. In this case, the buoyancy gradient can be written as a function of depth only and solved analytically to obtain an expression for the mixing power in terms of the boundary conditions:

$$P = g\kappa\left(\rho_0^* - \rho_h^*\right) \tag{4}$$

The second method accounts for the full nonlinear dependence of potential density on both potential temperature θ and salinity S by expressing the vertical derivative in (3) in terms of θ and S:

$$P = \int_0^h g\kappa\left(\frac{\partial\rho^*}{\partial\theta}\frac{d\theta}{dz} + \frac{\partial\rho^*}{\partial S}\frac{dS}{dz}\right)dz \tag{5}$$

This expression was integrated numerically over the spatial domain and averaged over one year at equilibrium to obtain an annual mean value for the total power expended in mixing over the entire basin for each run.

Table 1: Listing of key model parameters.

Key Model Parameters	
Parameter	**Value**
Domain size	60° longitude × 64° latitude × 4500 m deep
Southern boundary	Equator
Western boundary	0° longitude
Spatial resolution	3.75° longitude × 4° latitude ×16 vertical levels
Time step size	1 hour momentum, 24 hours tracers
Tracer restoring timescale	30 days
Background (pelagic) diffusivity	10^{-5} m^2/s
Wind stress	Time invariant zonal means based on Hellerman and Rosenstein (1981)

Table 2: Location of mixing for the two categories of experiments.

Mixing Location	
Experiment category	**Location of mixing**
Boundary mixing	All 60 grid columns adjacent to boundaries
Highly Localized mixing	Grid column cenetered at 10° N, 24.375° E

Table 3: Vertical diffusivities of tracers used in each model run. The time- and area-weighted diffusivity for latitudes 0° - 36° N was held constant across all runs, neglecting the pelagic diffusivity.

Vertical Tracer Diffusivities	
	Diffusivity during on state ($\times 10^{-4}$ m^2/s)
Boundary Mixing	
12 months on / 0 off	5
6 months on / 6 off	10
3 months on / 9 off	20
2 months on / 10 off	30
1 month on / 11 off	60
Highly localized mixing	
12 months on / 0 off	160
6 months on / 6 off	320
3 months on / 9 off	640
2 months on / 10 off	960
1 month on / 11 off	1920

Chapter 3

Results

3.1 Mass and Heat Transport

The annual mean overturning streamfunctions are displayed in figures 1 and 2 for each run in the two categories of experiments. Annual mean streamfunctions were used as the indicators of MOC strength because of the existence of transient behavior (discussed in greater detail below) with timescales of months that did not contribute to the annual mean mass transport. The streamfunctions for boundary mixing are almost identical, with a weak decrease in the strength of overturning as mixing transience increased. For highly localized mixing, the inverse relationship between overturning strength and mixing transience was stronger. Figure 3 depicts explicitly the relationship of the spatial maximum of the annual mean overturning to the degree of mixing transience. For boundary mixing runs, the weak inverse relationship between overturning and transience did not hold between the data points for 3 months/year and 2 months/year, but the relative magnitude of this deviation was so low (0.07%) that it was considered insignificant; numeric imprecision over the course of integration most likely contributes a greater uncertainty to these data points.

Figure 3 also shows that a given amount of mixing (i.e. a particular value of time- and area-weighted diapycnal diffusivity) produced less overturning when it was highly localized in space. This result was fully explored by Scott and Marotzke and will not be discussed here, as this study considered the effect of changes in mixing distribution in the time domain only.

When considered a function of mixing transience, the net meridional oceanic heat flux behaved similarly to the total mass transport. Heat transport was computed as an annual mean, zonally averaged function of latitude and is displayed in figure 4. The shape of the heat transport curve as a function of latitude does not vary significantly with mixing transience, at least at the spatial resolution used in this study.

The zonally- and meridionally-averaged heat flux was also plotted against overturning (figure 5) to provide a parametric representation, as a function of mixing

transience, of the efficiency of the MOC at transporting heat. For highly localized mixing, the heat flux average was taken over the whole basin as well as over latitudes north of the southern boundary of the mixing site; little difference was found between these two averages. As mixing transience varied, northward heat transport was found to be less sensitive to the strength of the overturning for the case of highly localized mixing. However, overturnings for the two categories of mixing had considerably different magnitudes, so it is possible that this sensitivity is correlated with the strength of the overturning and not the type of mixing.

3.2 Normalization by Power

Expressions (4) and (5) were evaluated numerically for each run and the results listed in table 4. Little difference was found between the values obtained from these two methods. The results of the nonlinear method (expression 5) are displayed in figure 6 and were used as the measure of mixing power in all subsequent analyses. As mixing transience increased in both categories of experiments, the power expended in mixing decreased considerably more quickly than the strength of the overturning. Thus, when the meridional transport of heat was normalized by power, highly transient mixing was shown to be more efficient at transporting heat (figure 7).

As mixing transience varied, the strength of the MOC was found to be more sensitive to mixing power for the case of highly localized mixing (figure 8). However, as was the case for the sensitivity of heat transport to overturning, a definite correlation between this sensitivity and the localization of mixing could not be established because of the different ranges of overturning and mixing power under consideration.

3.3 Detailed Dynamics

An inspection of the detailed dynamical behavior of one run will aid to illustrate the effect of mixing transience on circulation. Instantaneous plots of the overturning streamfunction (figure 9) are provided at several time points during one year at equilibrium for the case of boundary mixing of 2 months/year. The streamfunction plots show several prominent features:

i) The main overturning cell occupying the bulk of the longitudinal cross section remains approximately constant in its total mass transport but changes shape slightly throughout the year.

ii) The southern 10° of the cross section are subject to severe transient oscillations

The time evolution of the transient oscillations described in (ii) can be seen from plots of the maximum overturning as a function of time (figure 10). It is important to interpret these plots as displays of the time evolution of instantaneous velocities along streamlines; the sharp peaks indicate transitory oscillations that do not contribute to the annual mean transport of mass or heat. This was confirmed by calculation of the annual mean streamfunctions and heat transport provided in figures 1, 2, and 4.

Cross sections of the velocity and temperature fields at a time point during the mixing for boundary mixing of 2 months/year are provided in figure 11. The dynamics were similar to those discussed in detail by Scott and Marotzke with the addition of transient oscillations in the southern part of the basin. Upwelling occurred along the entire western and southern boundary walls, and sinking took place close to the northern boundary. Flow toward the east occurred in the top several hundred meters across the northern part of the basin, augmenting the downwelling in the northeast corner. A warm anomaly was apparently advected to the west away from the eastern boundary at a depth of about 1 km.

While differences in the detailed dynamics exist between the example case just discussed and other runs conducted in this study, the behavior seen in this run illustrates features common to all runs. The most striking dynamical variation between runs of different mixing transience was the frequency and magnitude of the transient oscillations, which can be seen in figure 10. Two to four oscillations occurred per year with significant damping. A plot of the velocity and temperature fields in the horizontal plane for the case of highly localized mixing of 2 months/year is provided in figure 12 for comparison. The location of the mixing column is easily discernible in the most shallow cross section, with temperatures 15° C colder than surrounding grid cells.

Table 4: Calculated values of annual mean power expended in mixing over one year at equilibrium. The linear calculation assumed potential density was a linear function of potential temperature, allowing power to be calculated from boundary conditions. The nonlinear calculation accounted for the full nonlinear dependence of potential density on potential temperature and salinity via the equation of state. All values were spatially integrated over the entire basin and included contributions by mixing due to pelagic diffusivity.

Annual Mean Power Expended in Mixing		
	Linear equation of state calculation ($\times 10^{10}$ W)	**Nonlinear equation of state calculation ($\times 10^{10}$ W)**
Boundary Mixing		
12 months on / 0 off	9.43	10.03
6 months on / 6 off	8.88	9.40
3 months on / 9 off	8.24	8.70
2 months on / 10 off	7.78	8.16
1 month on / 11 off	7.17	7.45
Highly localized mixing		
12 months on / 0 off	4.79	4.90
6 months on / 6 off	3.63	3.65
3 months on / 9 off	2.86	2.83
2 months on / 10 off	2.77	2.73
1 month on / 11 off	2.07	2.00

Chapter 4

Discussion

The strength of the MOC was insensitive to the transience of mixing when mixing was spatially diffuse (i.e. spread evenly over all boundary cells). When mixing was highly localized, with diapycnal diffusivity 32 times as great as the boundary mixing case, MOC strength decreased as the transience of mixing increased. However, this was a fairly weak relationship, as MOC mass transport decreased by 25% between the control case of time-invariant mixing and the most extreme case of mixing applied 1 month/year. Meridional heat transport displayed similar behavior.

The cause of the sensitivity of the MOC to transience in the case of highly localized mixing can be found in the restoring timescale for temperature, as discussed by Scott and Marotzke. Cases of highly localized mixing produce surface temperatures at the site of mixing 10-15° C lower than nearby grid columns without mixing, inhibiting the diffusion of heat into the thermocline. Scott and Marotzke showed that, for time-invariant highly localized mixing, decreasing the restoring timescale from 30 days to 2 days resulted in an increased overturning. Apparently, diffusivities used for boundary mixing, even in the most transient case, were low enough so as not to considerably inhibit the diapycnal diffusion of heat. The restoring timescale only became an issue when mixing was spatially concentrated with diffusivities 32 times as great as the boundary mixing cases.

One of the most notable effects of increasing mixing transience was the change in the transient behavior of circulation dynamics. As mixing transience increased, flow velocities in the entire depth of the basin in the tropics displayed complex, transient oscillatory behavior. Rossby and Kelvin waves are the mechanism by which the ocean responds to changes in buoyancy forcing; similar dynamics were likely involved in the transient response observed here. While the highly idealized nature of the model make it unlikely that this particular behavior would extend to real ocean circulation, it does suggest that some sort of transient response may occur if mixing took place on short

timescales. Data sets could be examined for evidence of transient response after suspected mixing events.

If mixing in real oceans does exhibit a significant degree of transience, it is possible that the global ensemble of transient mixing events could result in an overall distribution of mixing that is more stochastic and spatially diffuse than that modeled here. One example of this would be mixing induced by tropical cyclones. Tropical cyclones manifest on timescales of weeks with average translation speeds around 8 m/s. One parameterization of tropical cyclone mixing using the present model might apply mixing in one grid column for a timescale on the order of a week, then change the location of the mixing column. Pilot tests of such runs were begun in this study, but results were not fully analyzed. Preliminary findings suggest that the annual mean meridional transport of mass and heat was similar to that of highly localized mixing, with a stochastic transient response. The magnitude of these stochastic transient oscillations seemed to increase with the time the mixing column spent in one location before moving. It is possible to imagine, then, that a global simulation of diapycnal mixing with spatial and temporal behavior similar to that of tropical cyclones could produce MOC behavior similar to that of the highly localized runs with significant smoothing of transient response.

Questions remain regarding the relationship of MOC strength to the energy expended in mixing. As mixing transience increased, the annual mean mixing power decreased faster than the MOC transport of both mass and heat. This suggests the surprising result that, for a given quantity of energy available for diapycnal mixing, the strength of the overturning will increase with mixing transience. This leads one to question the accuracy of the power calculation—perhaps the numeric integration used to approximate power failed because the low time and spatial resolution of the model produced sufficient smoothing on integration to obscure nonlinearities that were more significant in highly transient cases. Repeating runs at higher resolutions would be a useful check.

It would also be useful to perform a set of runs where diffusivities were adjusted to produce similar values of overturning for the boundary and highly localized cases. It could then be determined if the sensitivities under consideration (that of heat flux to

overturning, displayed in figure 5, and that of overturning to mixing power, displayed in figure 8) were functions of the spatial distribution of mixing.

Chapter 5

Conclusions

The idealized simulations of this study show that the strength of the MOC is insensitive to the transience of diapycnal mixing when mixing is not highly localized in space. MOC strength became somewhat sensitive to mixing transience when the mixing was highly localized in space, such that mass and heat transport decreased by about 20% when mixing transience increased by a factor of 10. This sensitivity is likely to be a strong function of the temperature restoring timescale.

The circulation dynamics displayed large-scale oscillations indicative of Rossby and Kelvin waves that increased in amplitude with mixing transience. Analogues in the real ocean might serve as indicators of highly transient mixing.

Attempts were made to quantify the relationship between mixing transience, MOC strength, and the power expended in mixing, and led to the unexpected result that for a given quantity of energy available for mixing, highly transient mixing produces a stronger overturning. Further investigation is needed to understand the model dynamics surrounding this result.

References

Emanuel, K., 2001. Contribution of tropical cyclones to meridional heat transport by the oceans. *J. Geophys. Res.*, **106**, 14,771-14,781.

Emanuel, K. Anthropogenic Effects on Tropical Cyclone Activity. Available on website http://www-paoc.mit.edu/~emanuel/home.html.

Emanuel, K. A., 2002. A simple model of multiple climate regimes. *J. Geophys. Res.*, submitted.

Faller, A. J., 1968. Sources of energy for the ocean circulation and a theory of the mixed layer. *Proceedings of the Fifth U.S. Congress of Applied Mechanics*. American Society of Mechanical Engineers, held at University of Minnesota, Minneapolis, 14-17 June 1966, 651-672.

Hall, M. M., and H. Bryden, 1982. Direct estimates and mechanism of ocean heat transport. *Deep Sea Res.*, **29**, 339-359.

Hartmann, D. L., 1994. *Global Physical Climatology*. Academic Press. 197-199.

Hellerman, S., and M. Rosenstein, 1983. Normal monthly wind stress over the world ocean with error estimates, *J. Phys, Oceanogr.*, **13**, 1093-1104.

Huang, R. X., 1999. Mixing and energetics of the oceanic thermohaline circulation. *J. Phys. Oceanogr.*, **29**, 727-746.

Jeffreys, H., 1925. On fluid motions produced by differences of temperature and humidity. *Quarterly Journal of the Royal Meteorological Society*, **51**, 347-356.

Macdonald, A. M., and C. Wunsch, 1996. The global ocean circulation and heat flux. *Nature*, **382**, 436-439.

Marotzke, J. and J. R. Scott, 1999. Convective mixing and the thermohaline circulation. *J. Phys. Oceanogr.*, **29**, 2962-2970.

Munk, W., and C. Wunsch, 1998. Abyssal recipes, II: Energetics of tidal and wind mixing. *Deep Sea Res.*, **45**, 1977-2010.

Oort, A. H., L. A. Anderson, and J. P. Peixoto, 1994. Estimates of the energy cycle of the oceans. *Journal of Geophysical Research*, **99**, 7665-7688.

Osborn, T. R. and C. S. Cox, 1972. Oceanic fine structure. *Geophysical Fluid Dynamics*, **3**, 321-345.

Pacanowski, R. C., 1996. *MOM 2 (Version 2.0 Beta) Documentation, User's Guide, and Reference Manual.* GFDL Ocean Technical Report 3.2, Geophysical Fluid Dynamics Laboratory/NOAA, Princeton, NJ. [Available from GFDL/NOAA, Princeton University, P.O. Box 308, Princeton, NJ 08542.]

Polzin, K. L., J. M. Toole, R. H. Schmitt, 1995. Finescale parameterizations of turbulent dissipation. *Journal of Physical Oceanography*, **25**, 306-328.

Polzin, K. L., J. M. Toole, J. R. Ledwell, and R. W. Schmitt, 1997. Spatial variability of turbulent mixing in the abyssal ocean. *Science*, **276**, 93-96.

Sandström, J. W., 1908. *Dynamische Versuche mit Meerwasser. Annals in Hydrodynamic Marine Meteorology*, **36**, 6-23.

Scott, J. R., and J. Marotzke, 2001. The location of diapycnal mixing and the meridional overturning circulation. *J. Phys. Oceanogr.*, submitted.

Trenberth, K. E., J. M. Caron, and D. P. Stepaniak, 2000. The atmospheric energy budget and implications for surface fluxes and ocean heat transports. *Clim. Dyn.*, **17**, 259-276.

a)

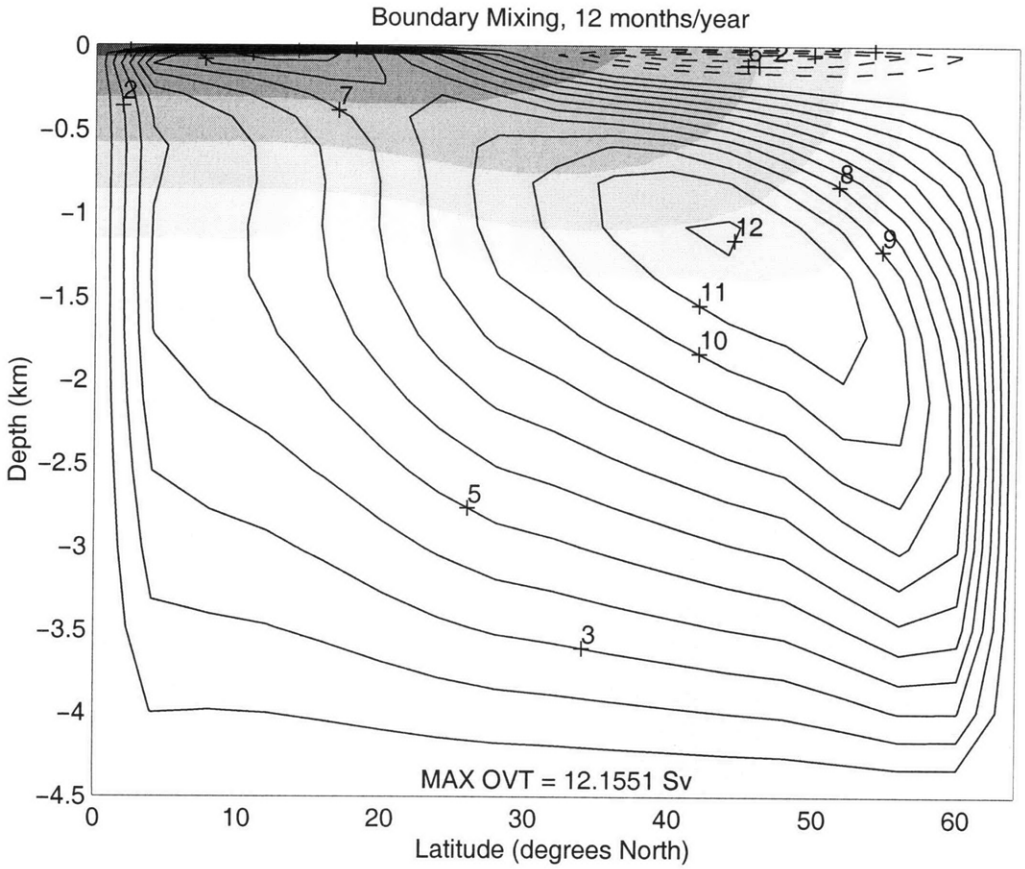

Figure 1: (a) – (e) are annual mean overturning streamfunctions for the boundary mixing case. The mean was taken over one year at equilibrium. Each plot corresponds to a different degree of mixing transience. Contours represent MOC mass transport with an interval of 1.0 Sverdrup. Shading represents temperature with the contour intervals set at 80%, 40%, 20%, 10%, and 5% of the approximate surface-to-bottom temperature differential of 27° C. The maximum overturning value (MAX OVT) is indicated on each plot.

b)

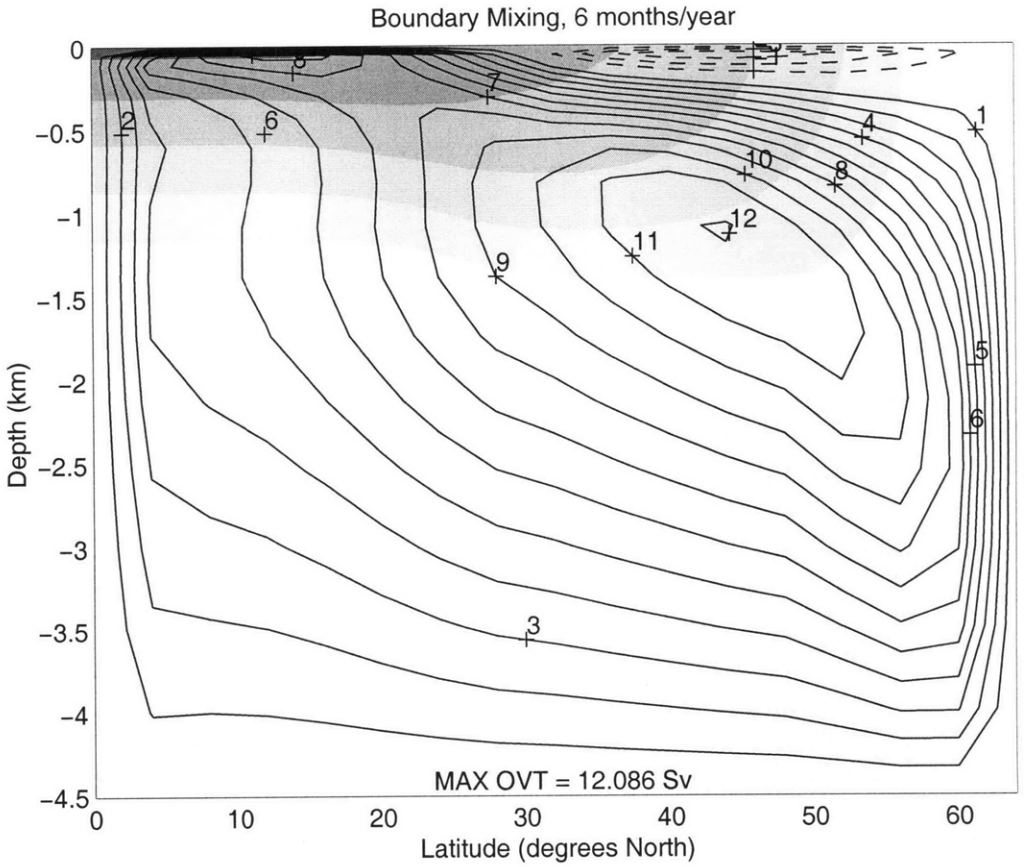
Boundary Mixing, 6 months/year
Depth (km)
Latitude (degrees North)
MAX OVT = 12.086 Sv
0
−0.5
−1
−1.5
−2
−2.5
−3
−3.5
−4
−4.5
0
10
20
30
40
50
60

c)

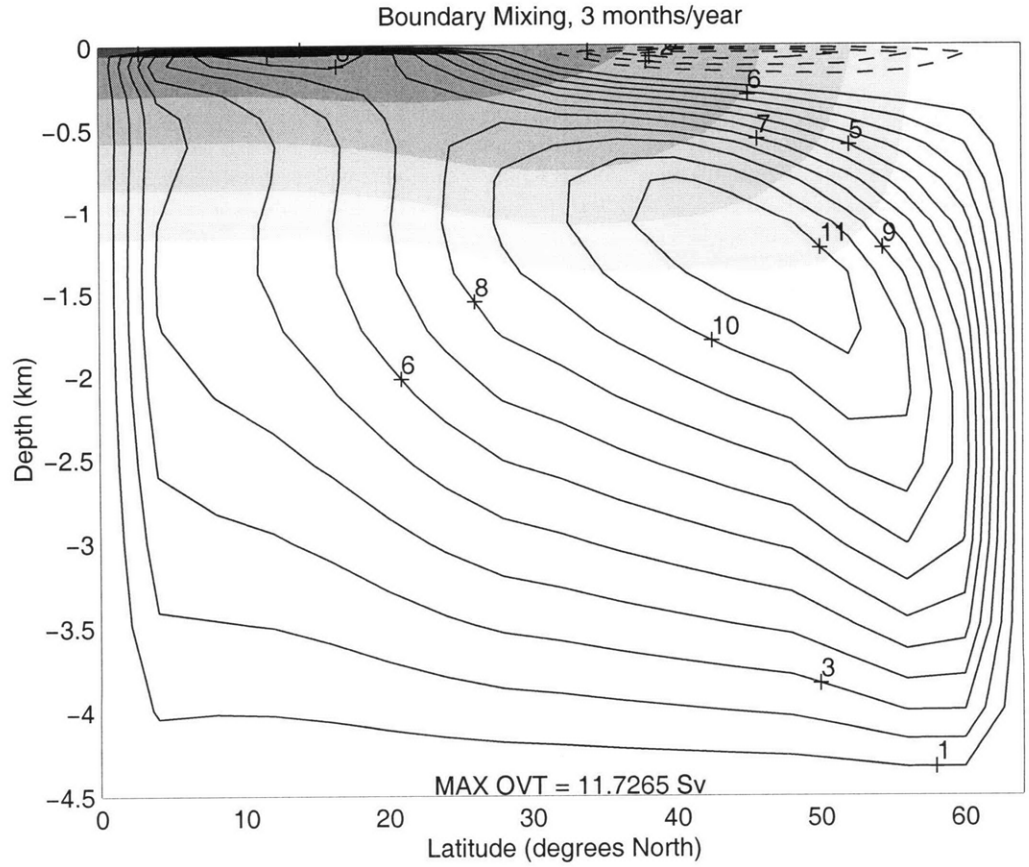
Boundary Mixing, 3 months/year
Depth (km)
Latitude (degrees North)
MAX OVT = 11.7265 Sv
0
−0.5
−1
−1.5
−2
−2.5
−3
−3.5
−4
−4.5
0
10
20
30
40
50
60

d)

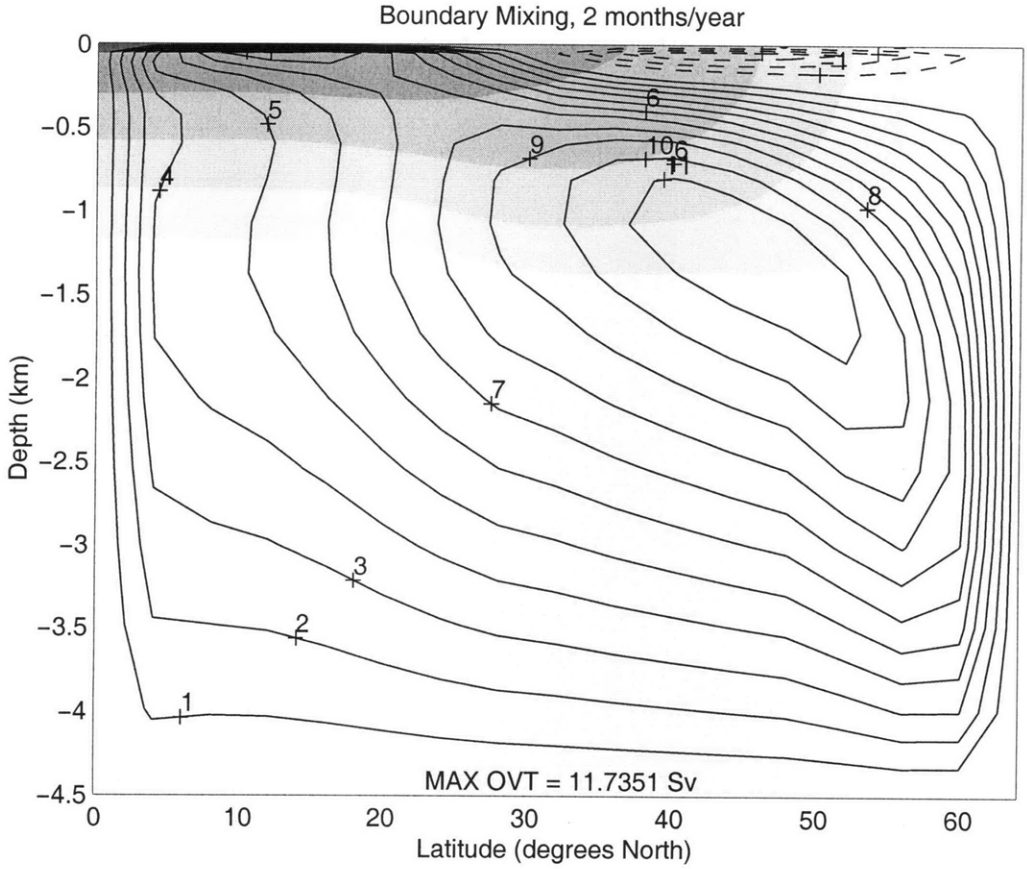
Boundary Mixing, 2 months/year
Depth (km)
Latitude (degrees North)
MAX OVT = 11.7351 Sv
0
-0.5
-1
-1.5
-2
-2.5
-3
-3.5
-4
-4.5
0
10
20
30
40
50
60
1
2
3
4
5
6
7
8
9
10
11

e)

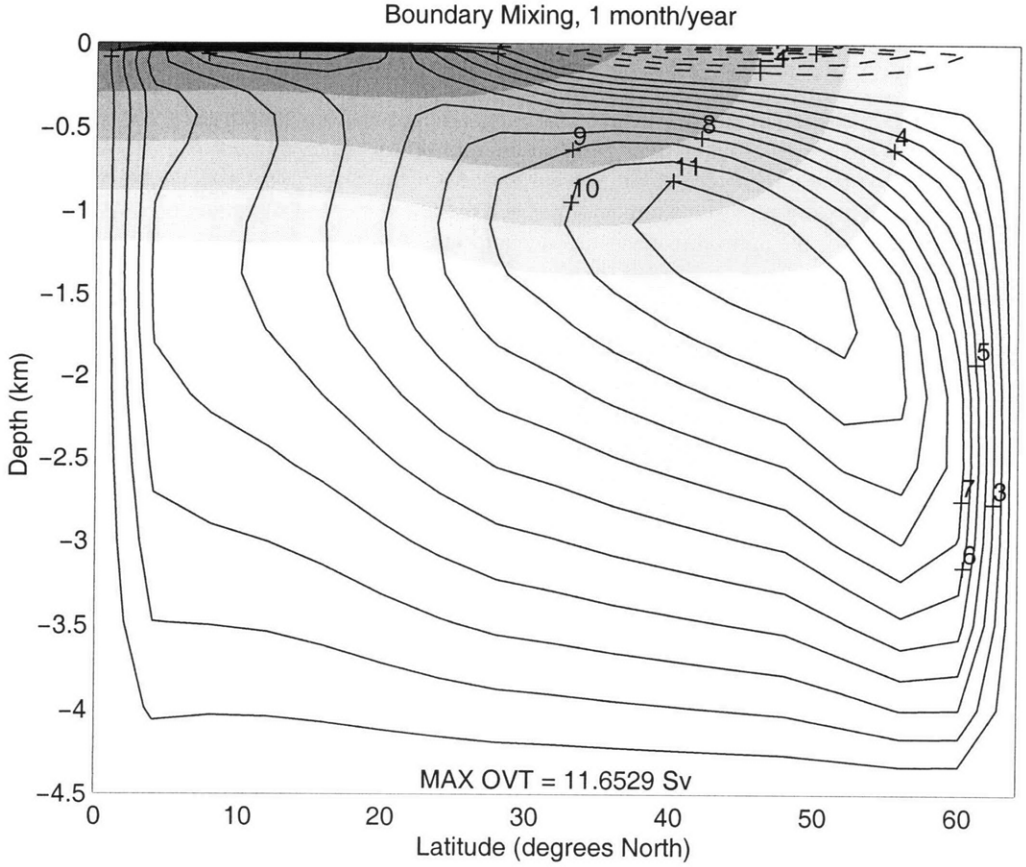
Boundary Mixing, 1 month/year
Depth (km)
Latitude (degrees North)
MAX OVT = 11.6529 Sv
0
-0.5
-1
-1.5
-2
-2.5
-3
-3.5
-4
-4.5
0
10
20
30
40
50
60
1
2
3
4
5
6
7
8
9
10
11

a)

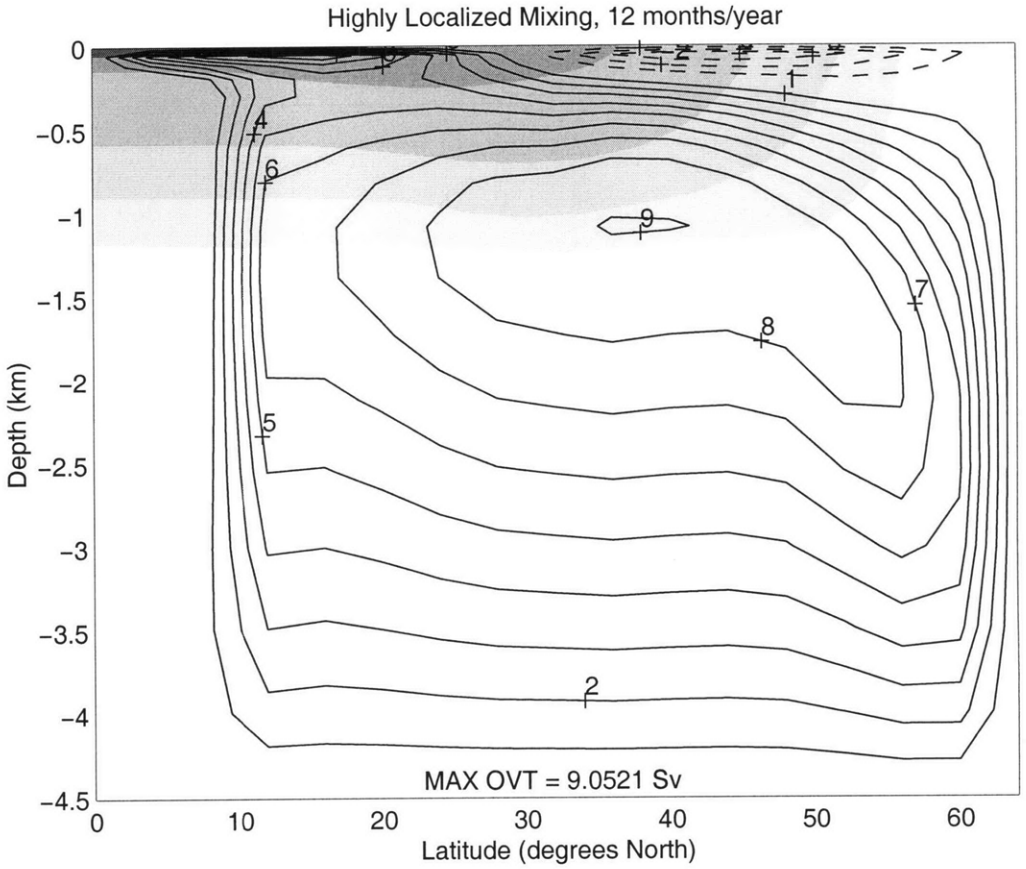

Figure 2: (a) – (e) are annual mean overturning streamfunctions for the case of highly localized mixing. The mean was taken over one year at equilibrium. Each plot corresponds to a different degree of mixing transience. Contours represent MOC mass transport with an interval of 1.0 Sverdrup. Shading represents temperature with the contour intervals set at 80%, 40%, 20%, 10%, and 5% of the approximate surface-to-bottom temperature differential of 27° C. The maximum overturning value is indicated on each plot.

b)

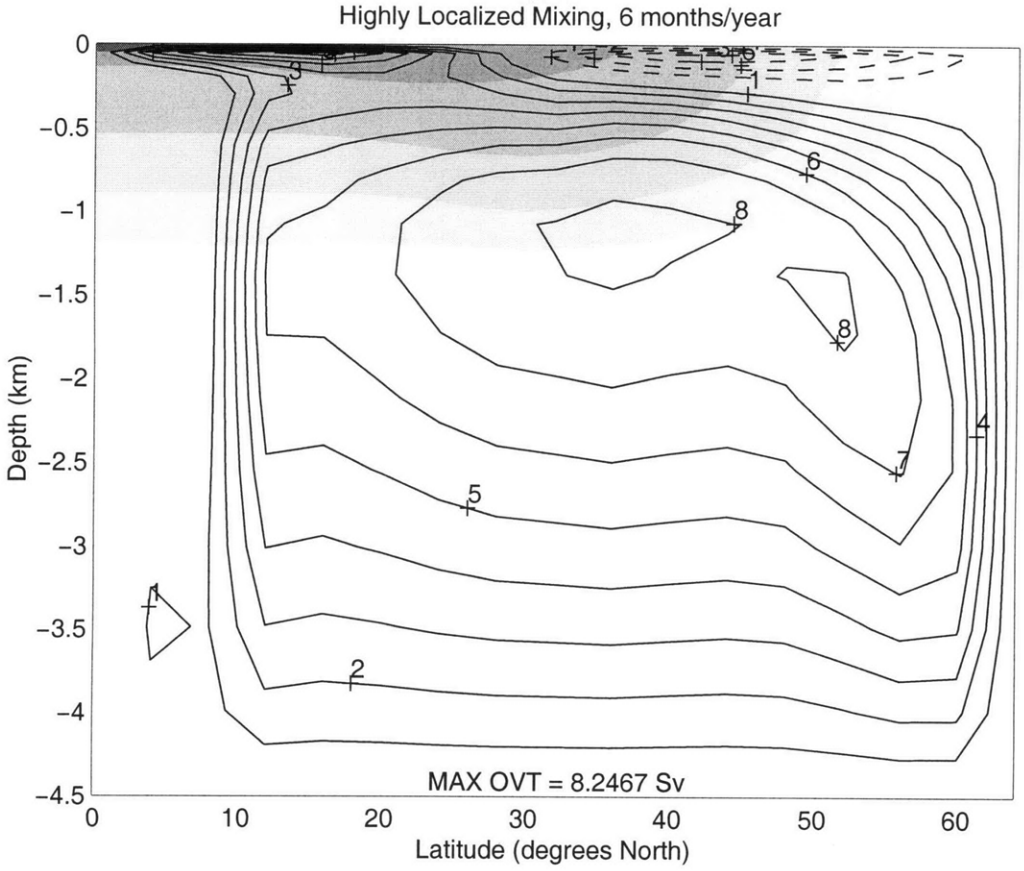
Highly Localized Mixing, 6 months/year
Depth (km)
Latitude (degrees North)
MAX OVT = 8.2467 Sv

c)

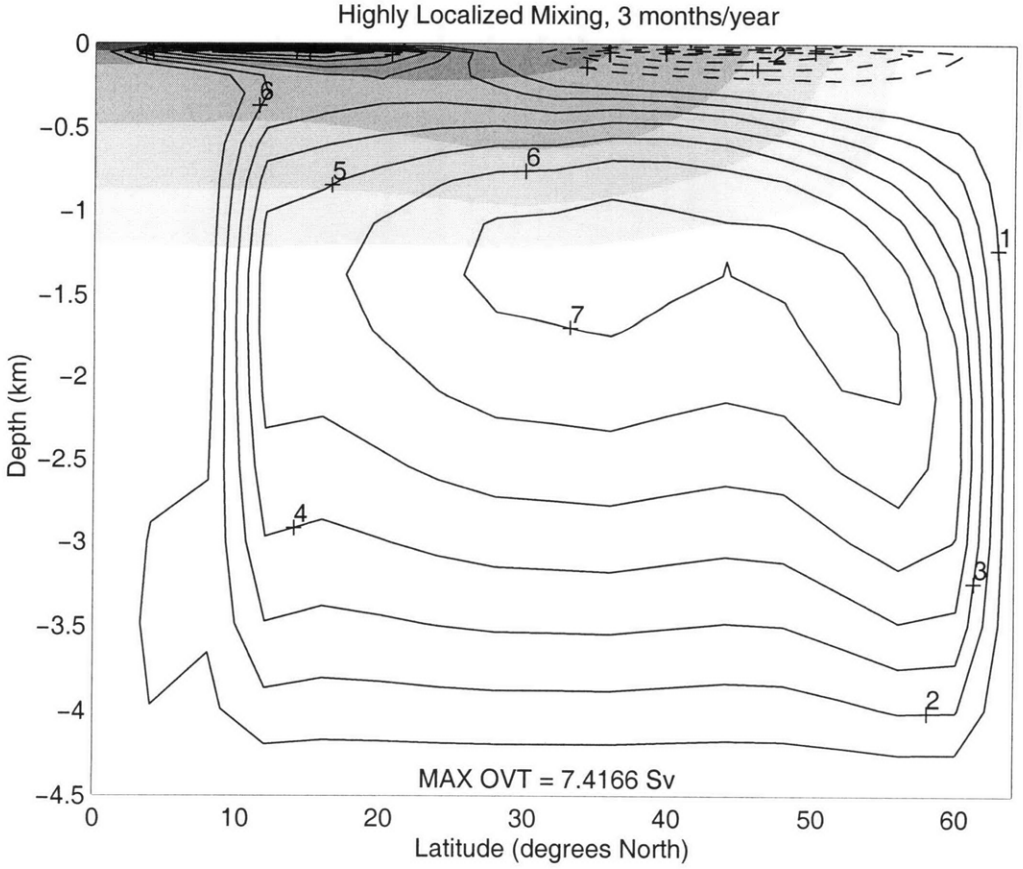
Highly Localized Mixing, 3 months/year
Depth (km)
Latitude (degrees North)
MAX OVT = 7.4166 Sv

d)

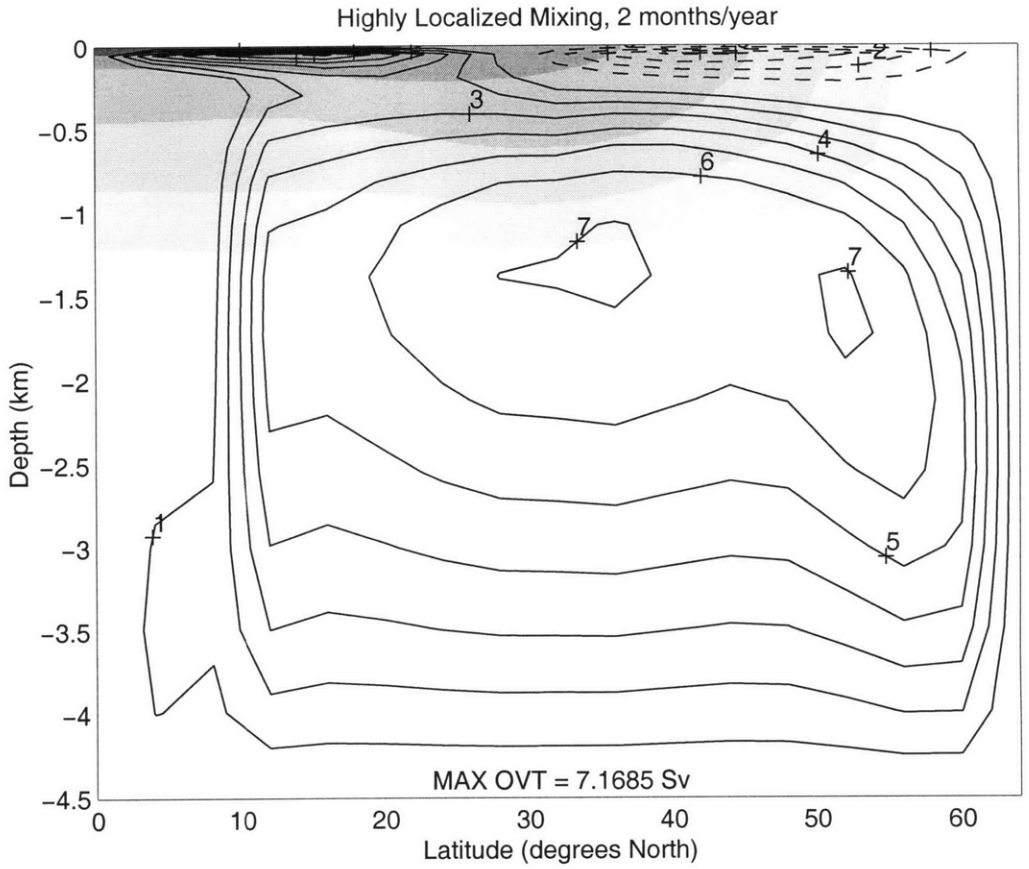
Highly Localized Mixing, 2 months/year
Depth (km)
Latitude (degrees North)
MAX OVT = 7.1685 Sv

e)

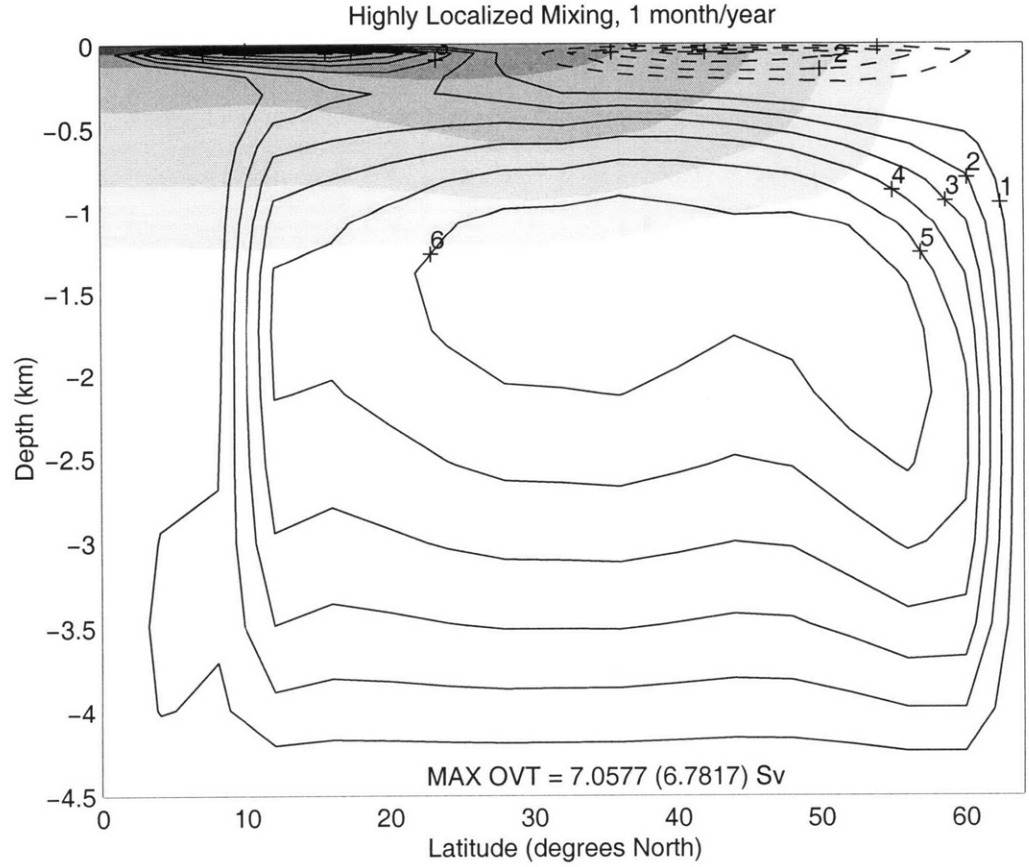
Highly Localized Mixing, 1 month/year
Depth (km)
Latitude (degrees North)
MAX OVT = 7.0577 (6.7817) Sv

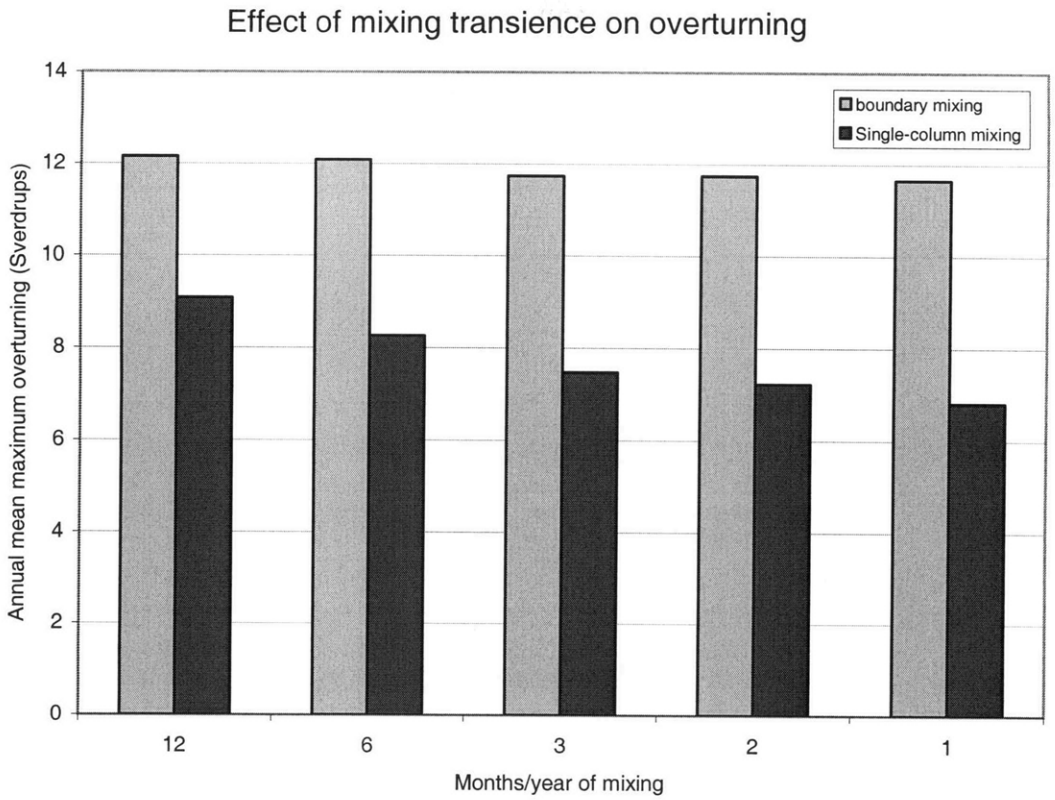

Figure 3: The effect of mixing transience on the spatial maximum of the annual mean overturning during one year at equilibrium.

Figure 4: Zonally-averaged, annual-mean northward oceanic heat flux as a function of latitude for one year at equilibrium. Curves follow the order given in the legend, from top to bottom.

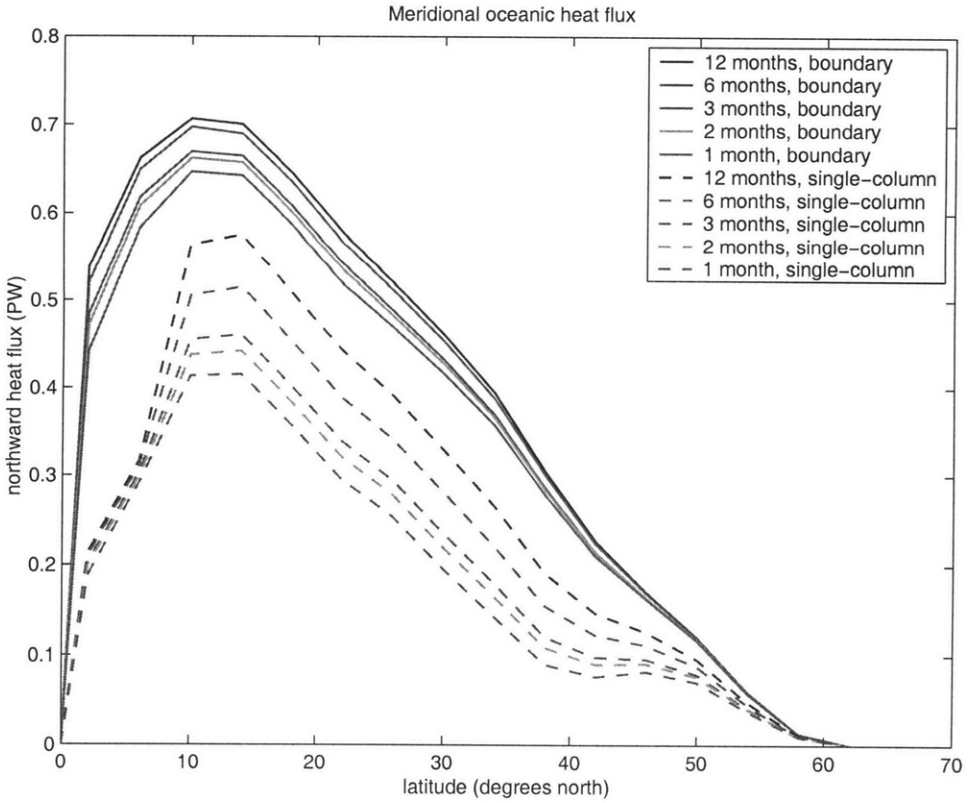

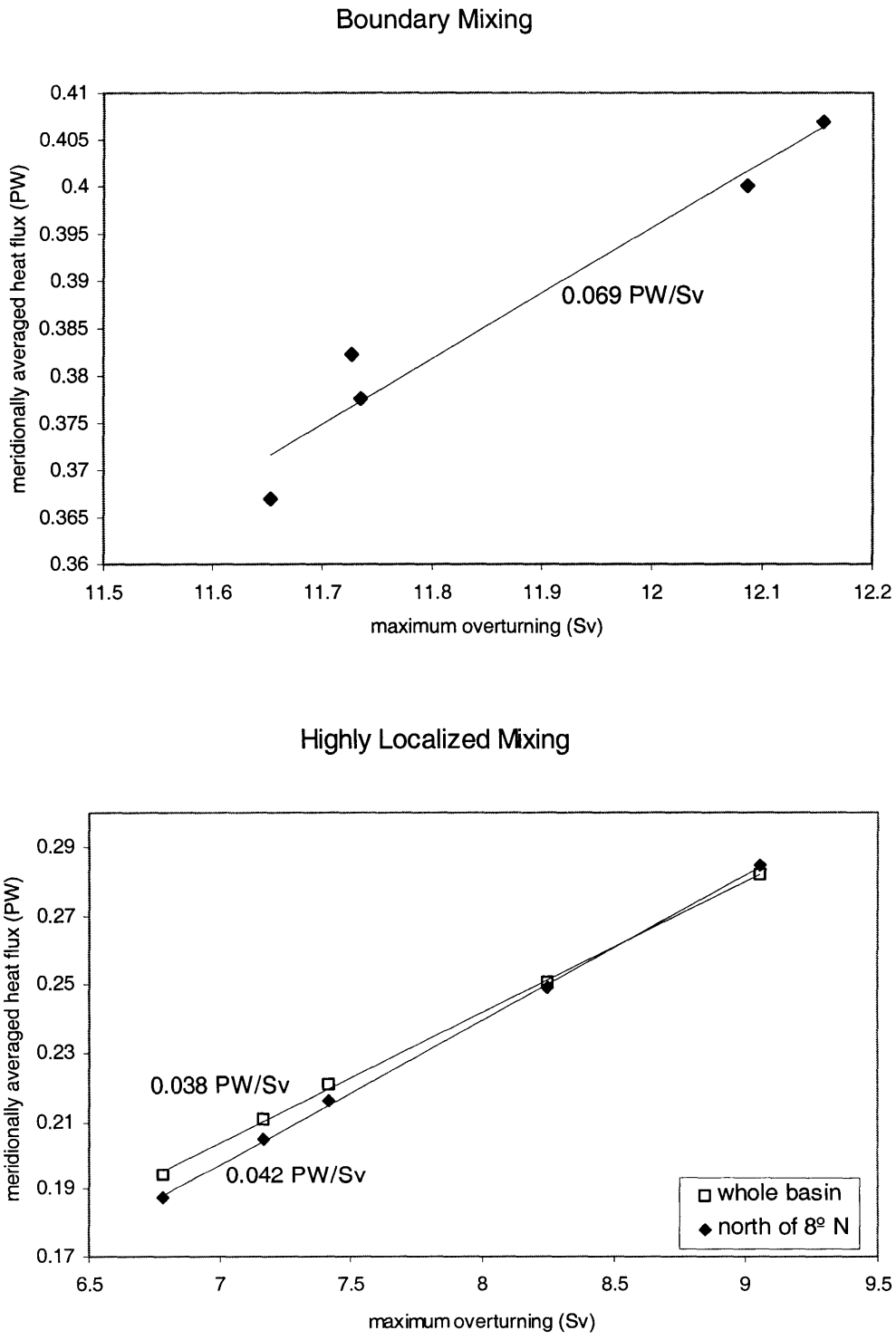

Figure 5: The relation of zonally- and meridionally-averaged oceanic heat flux to the spatial maximum of overturning. All data are mean values over one year at equilibrium. The data for latitudes north of 8° N in the case of highly localized mixing are provided to exclude regions south of the mixing column from the average. Slopes of the best linear least-squares fits are noted on the plots.

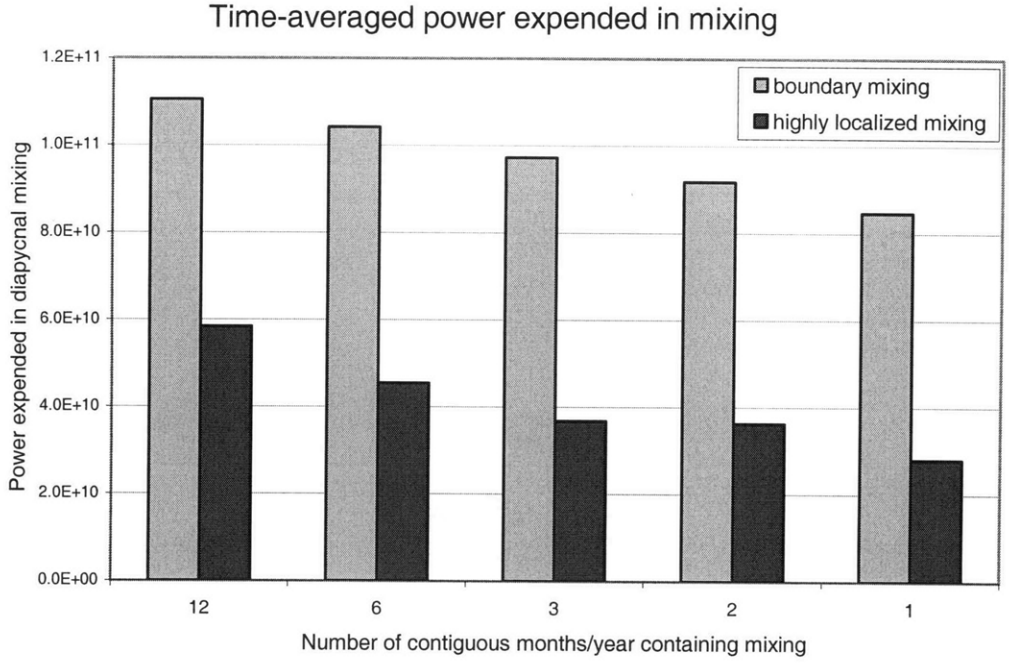

Figure 6: Annual mean, spatially integrated power expended in diapycnal mixing in one year at equilibrium, calculated using the full nonlinear dependence of potential density on temperature and salinity.

Figure 7: Zonally-averaged, annual-mean northward oceanic heat flux as a function of latitude for one year at equilibrium, normalized by power expended in diapycnal mixing relative to the control run of boundary mixing for 12 months/year. Curves follow the order given in the legend, from top to bottom.

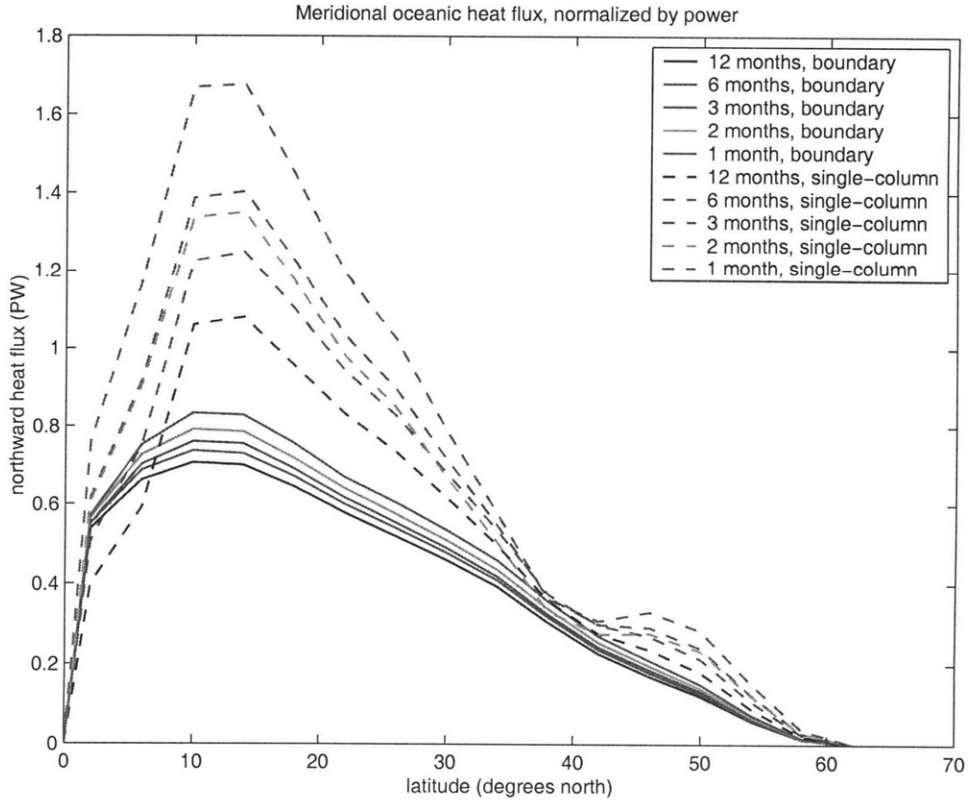

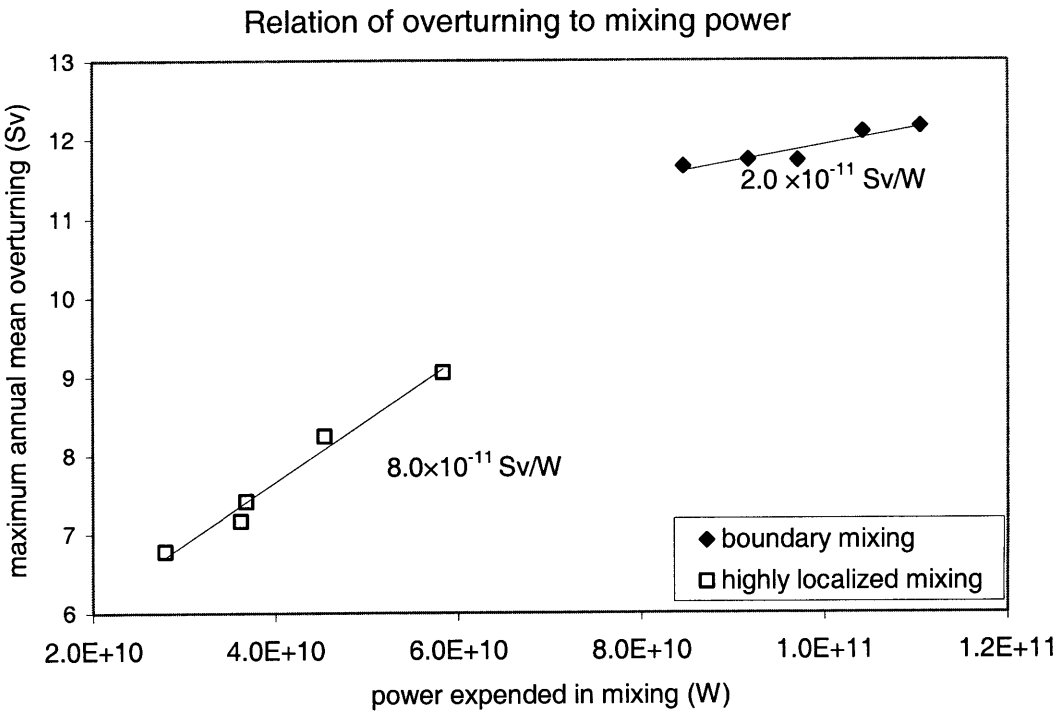

Figure 8: Relation of the spatial maximum of the annual mean overturning to the annual mean power expended in diapycnal mixing. Power values were calculated using the nonlinear dependence of potential density on temperature and salinity.

a)

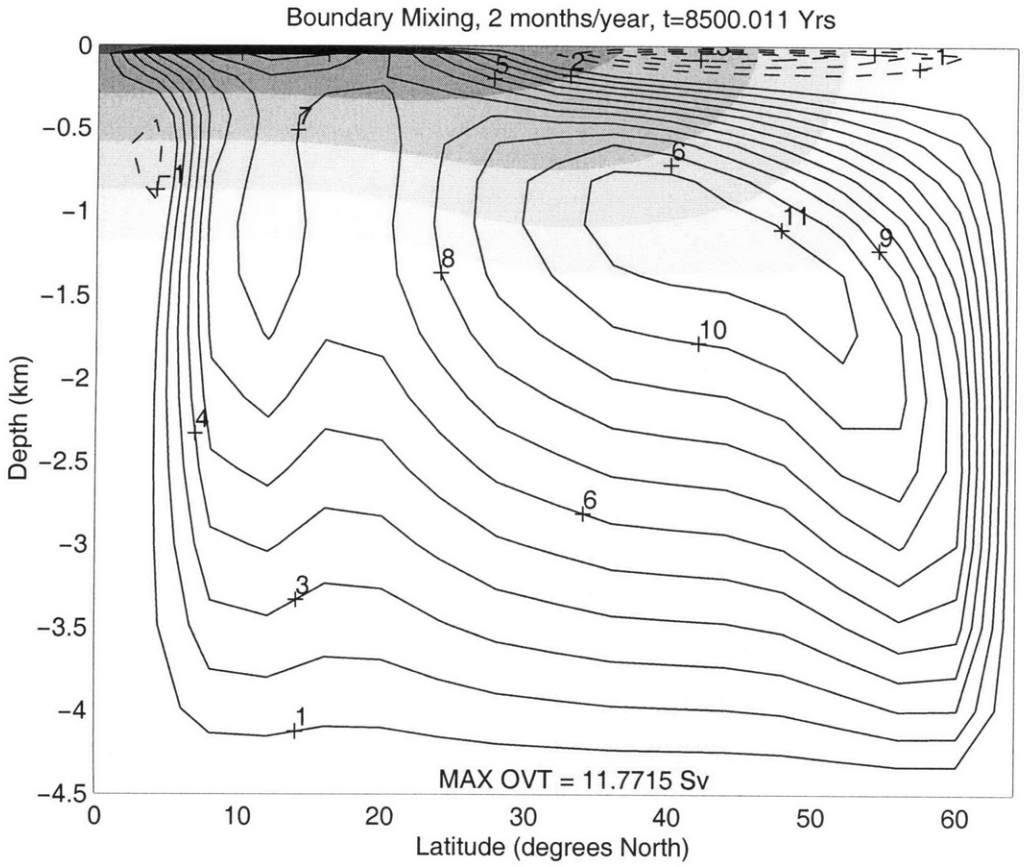

Figure 9: (a) – (d) are instantaneous overturning streamfunctions at 4 equally spaced and sequential times in one year at equilibrium for the case of boundary mixing of 2 months/year. Plot **(c)** represents the state of the model in the middle of the 2 months of mixing. Contours lines represent MOC mass transport with an interval of 1.0 Sverdrup. Solid contours indicate forward (clockwise) flow, while dashed contours indicate reverse flow. Shading represents temperature with the contour intervals set at 80%, 40%, 20%, 10%, and 5% of the approximate surface-to-bottom temperature differential of 27° C. The maximum overturning (MAX OVT) is indicated on each plot.

b)

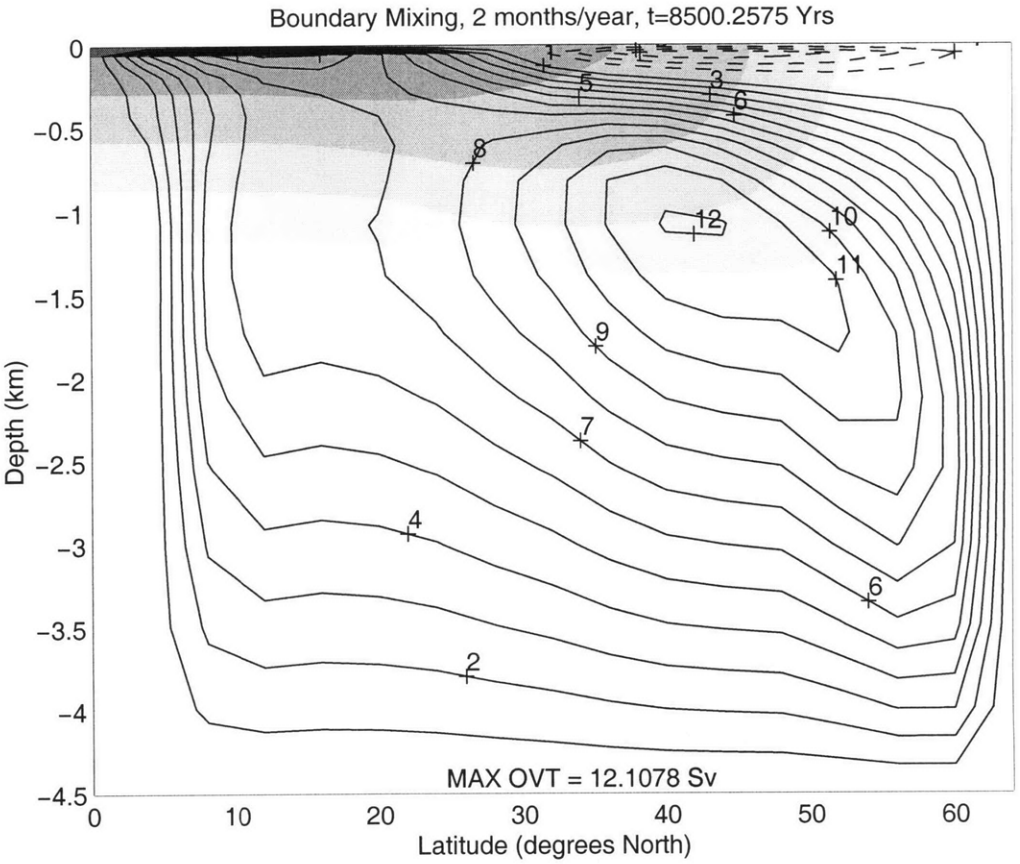
Boundary Mixing, 2 months/year, t=8500.2575 Yrs
Depth (km)
Latitude (degrees North)
MAX OVT = 12.1078 Sv
0
−0.5
−1
−1.5
−2
−2.5
−3
−3.5
−4
−4.5
0
10
20
30
40
50
60

c)

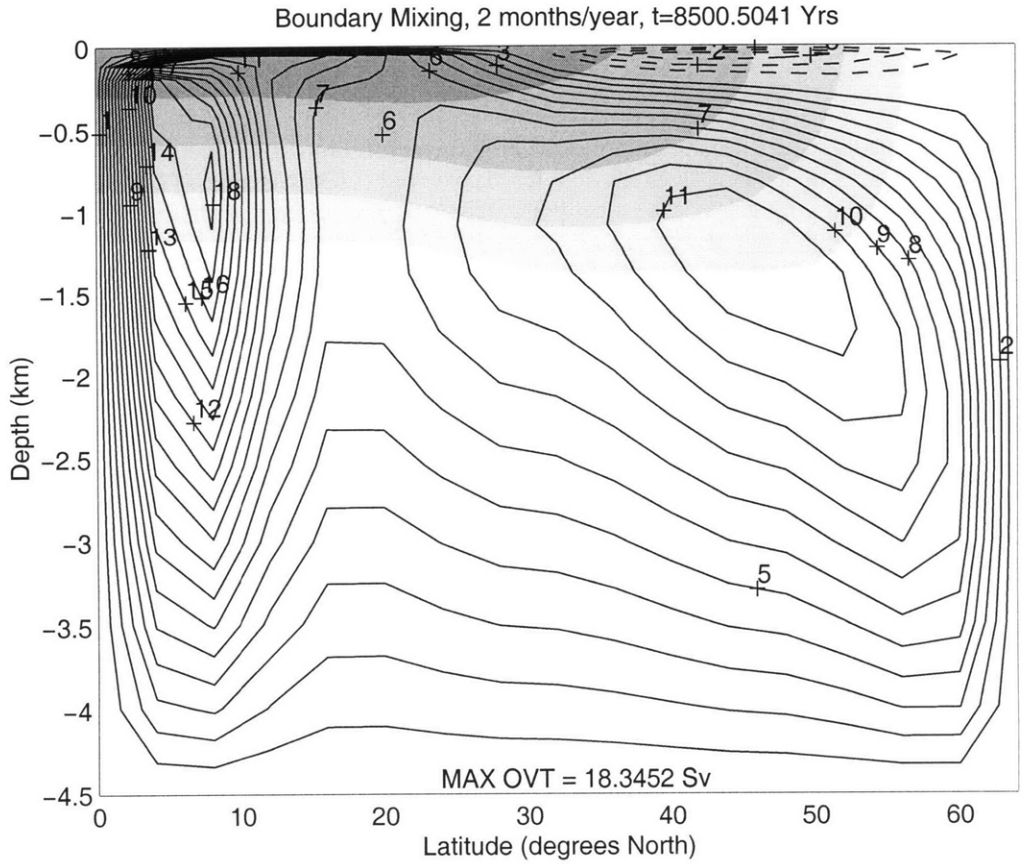
Boundary Mixing, 2 months/year, t=8500.5041 Yrs
Depth (km)
Latitude (degrees North)
MAX OVT = 18.3452 Sv
0
−0.5
−1
−1.5
−2
−2.5
−3
−3.5
−4
−4.5
0
10
20
30
40
50
60

d)

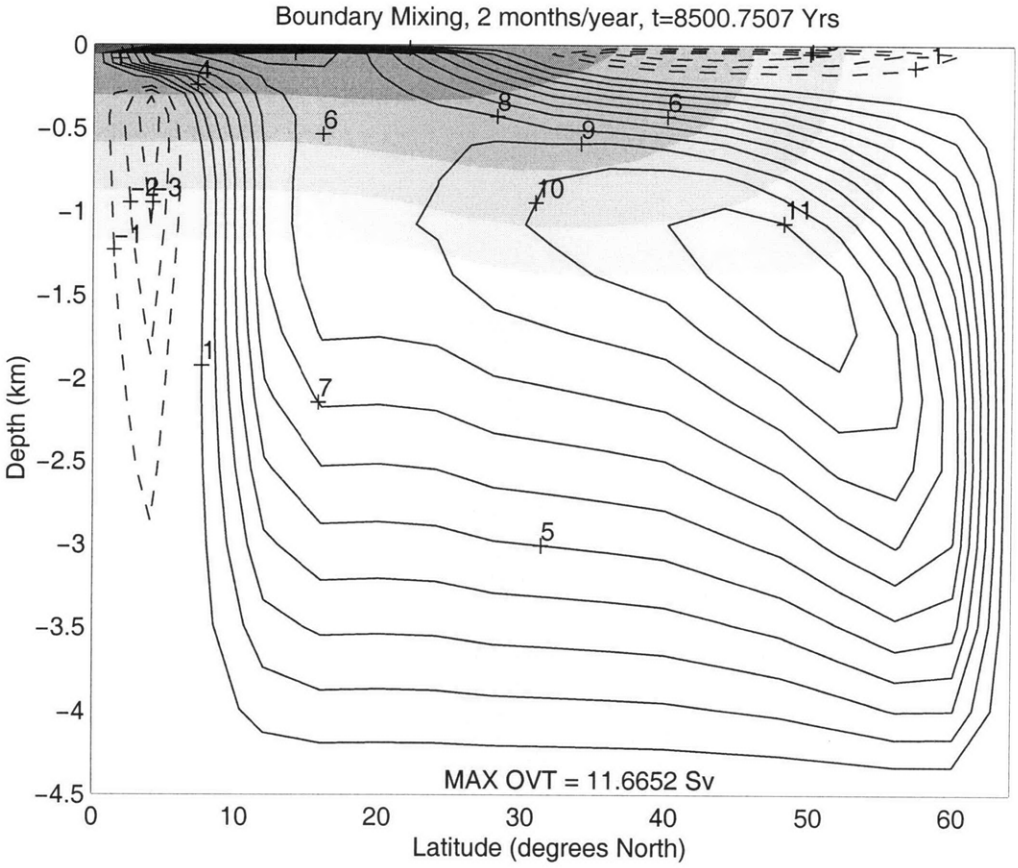
Boundary Mixing, 2 months/year, t=8500.7507 Yrs
Depth (km)
Latitude (degrees North)
MAX OVT = 11.6652 Sv
0
-0.5
-1
-1.5
-2
-2.5
-3
-3.5
-4
-4.5
0
10
20
30
40
50
60

Boundary Mixing

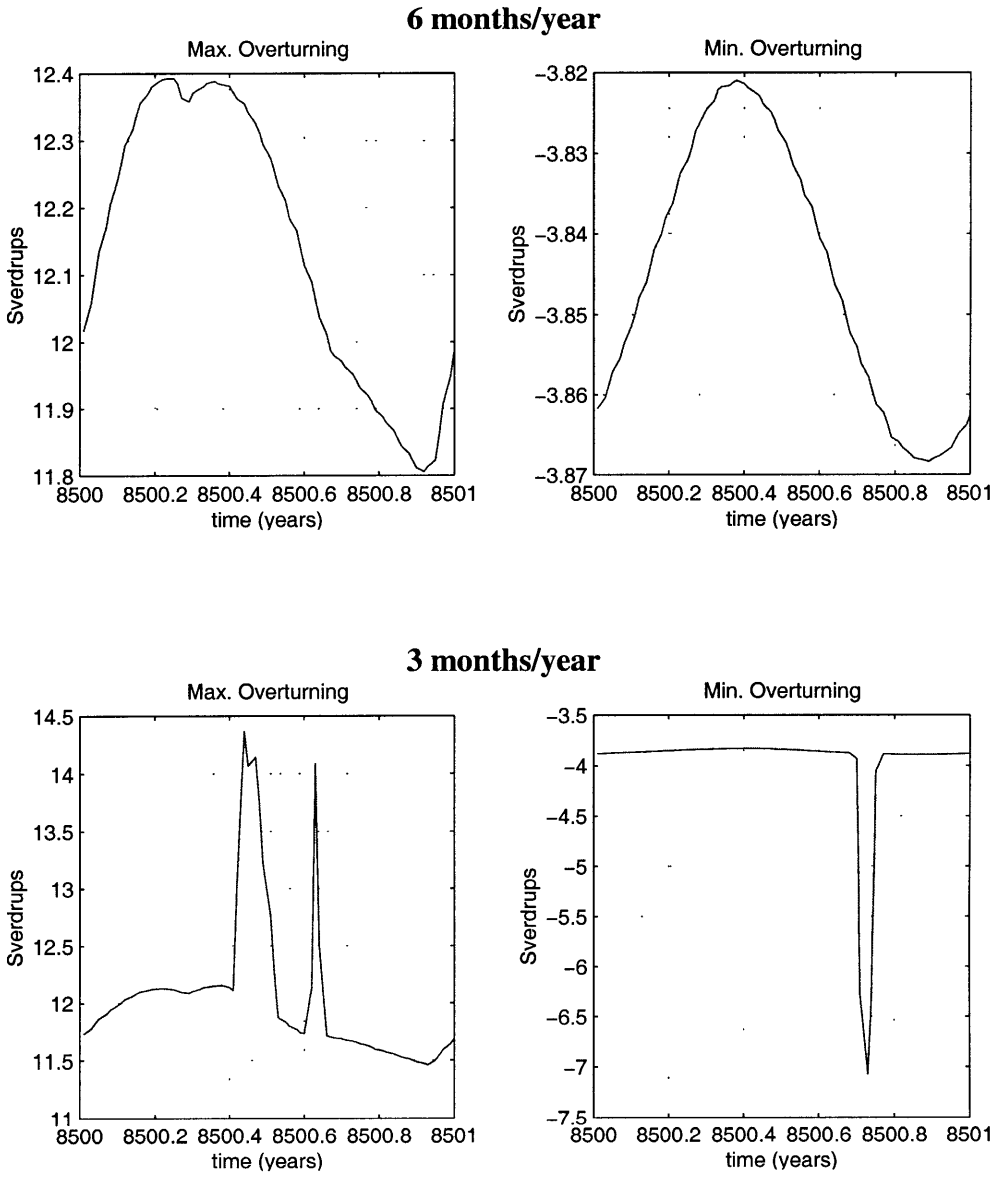

Figure 10: Plots on this page and the next 3 pages display time evolution of the instantaneous maximum and minimum overturning for each run over one year at equilibrium. The control cases of mixing for 12 months/year are not shown since these are horizontal lines with the values given in figures **1a** and **2a**. Note that the negative minimum overturning represents reverse velocities (equatorward at the surface and poleward at depth). Velocities were sampled once every 5 days.

Boundary Mixing (continued)

2 months/year

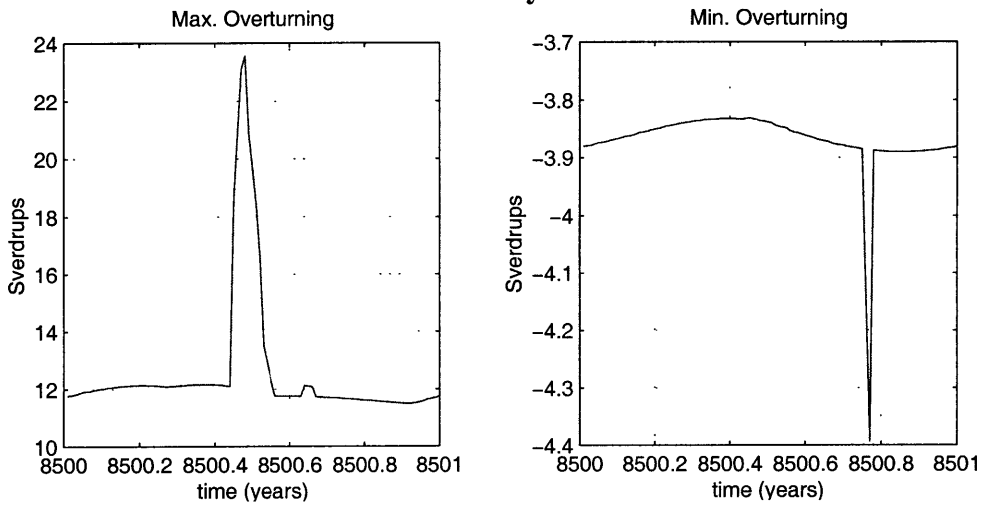

1 month/year

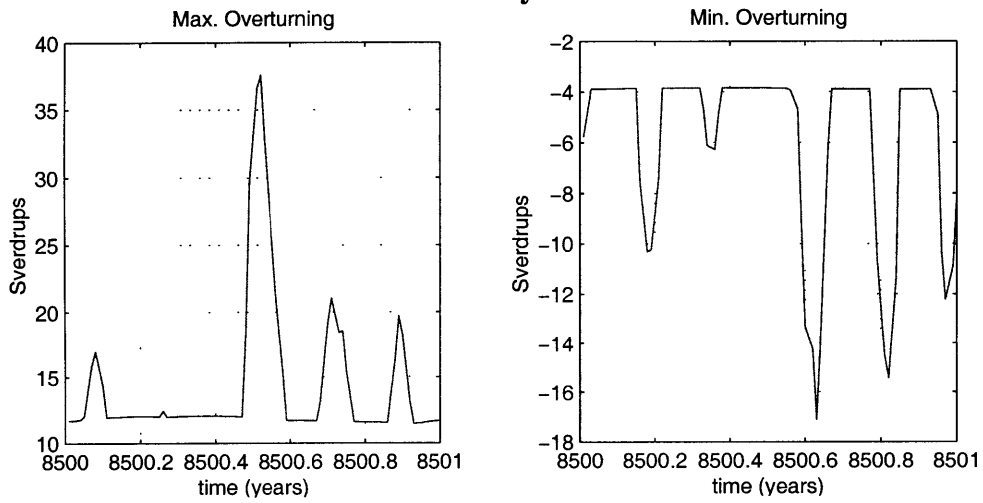

Highly Localized Mixing

6 months/year

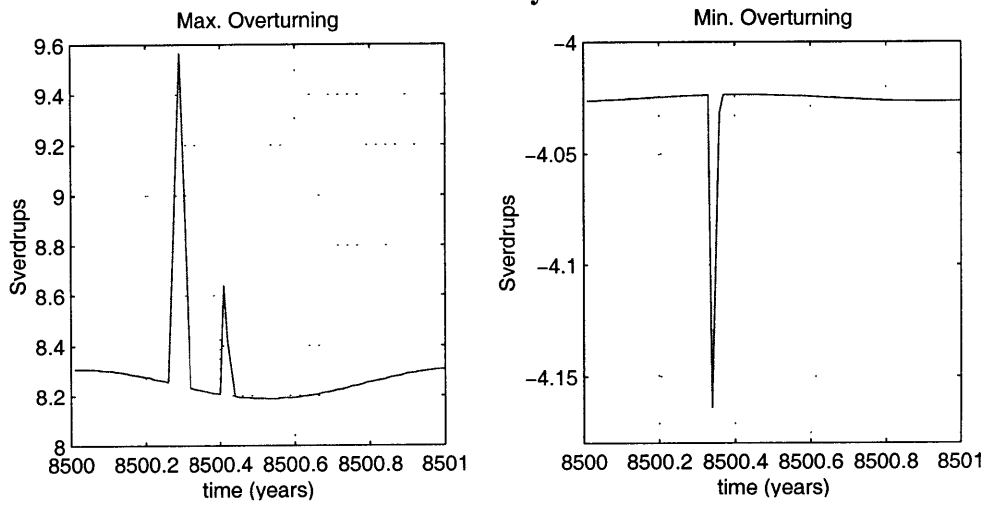

3 months/year

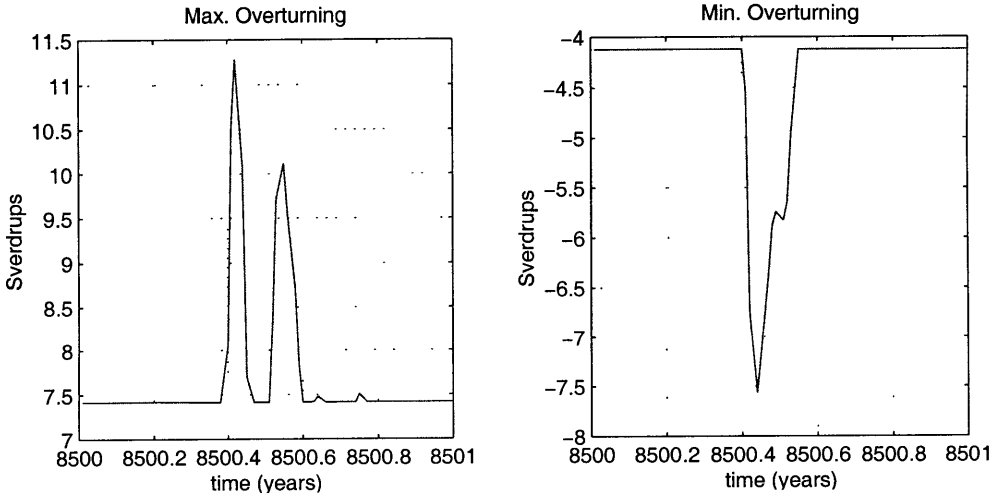

Highly Localized Mixing (continued)

2 months/year

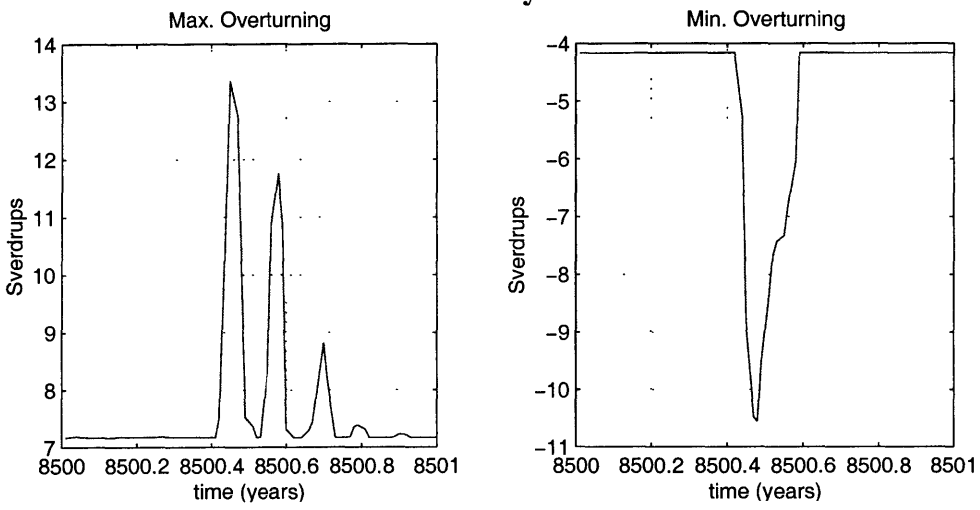

1 month/year

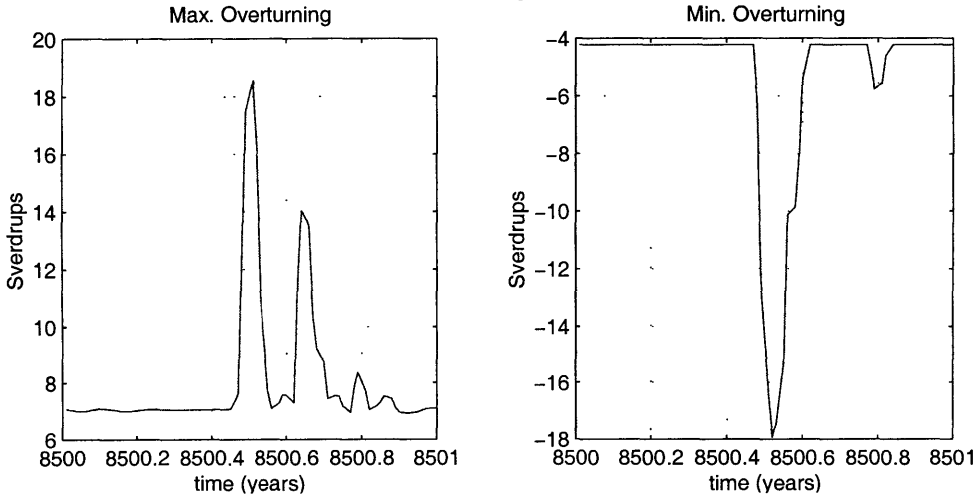

a)

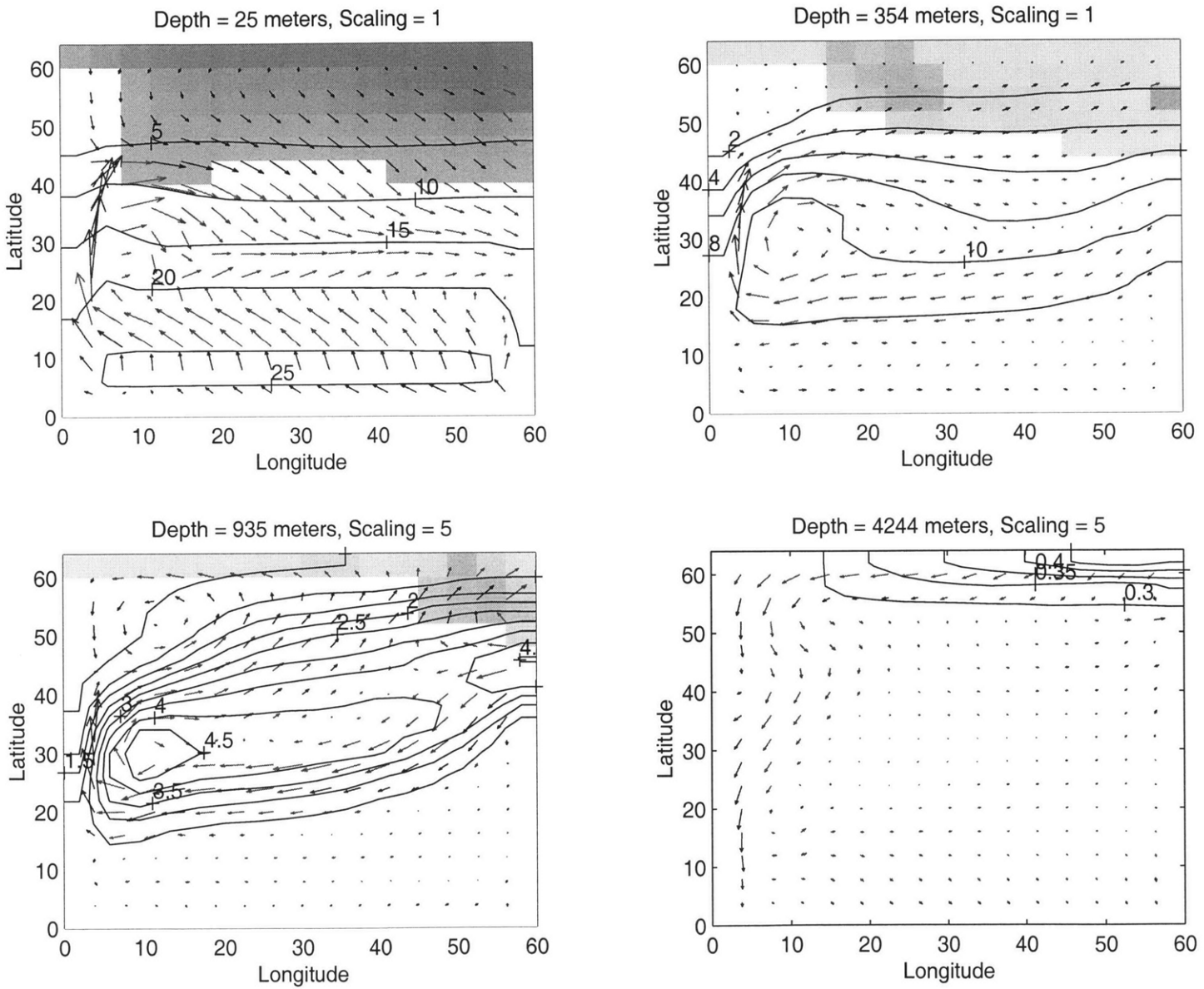

Figure 11: Velocity and temperature fields for the case of boundary mixing of 2 months/year. All plots represent the state of the system at the midpoint of the 2 months of mixing. Solid contours indicate temperature. Arrows indicate fluid velocities. Convection is shown by shading, with the degree of shading indicating the time rate of change of temperature due to convection. **(a)** is a horizontal cross section, **(b)** is zonal, and **(c)** is longitudinal.

b)

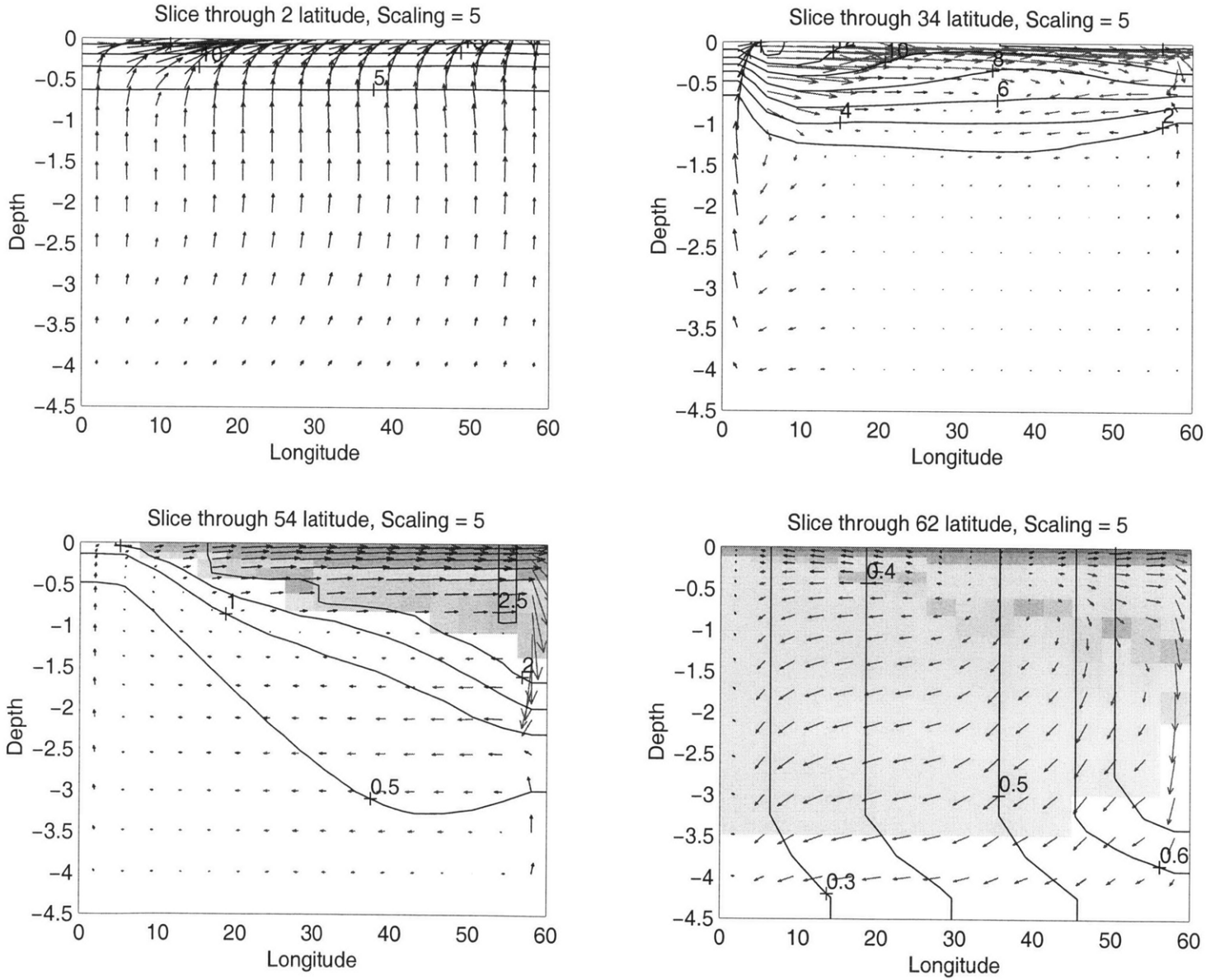
Slice through 2 latitude, Scaling = 5
Slice through 34 latitude, Scaling = 5
Slice through 54 latitude, Scaling = 5
Slice through 62 latitude, Scaling = 5
Depth
Longitude
0
-0.5
-1
-1.5
-2
-2.5
-3
-3.5
-4
-4.5
0
10
20
30
40
50
60
0.5
1
2
2.5
4
6
8
10
0.3
0.4
0.6

c)

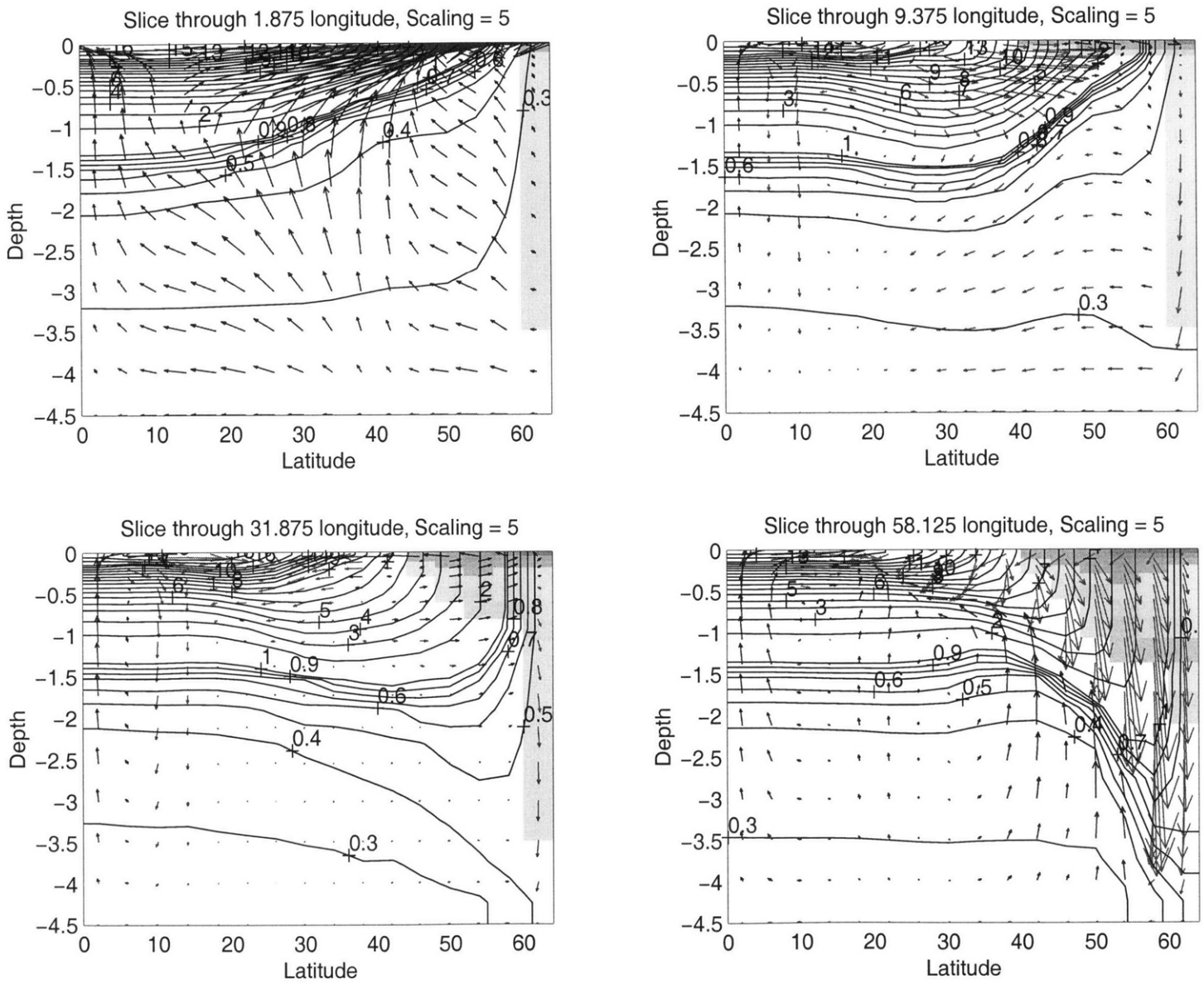
Slice through 1.875 longitude, Scaling = 5
Slice through 9.375 longitude, Scaling = 5
Slice through 31.875 longitude, Scaling = 5
Slice through 58.125 longitude, Scaling = 5
Depth
Latitude

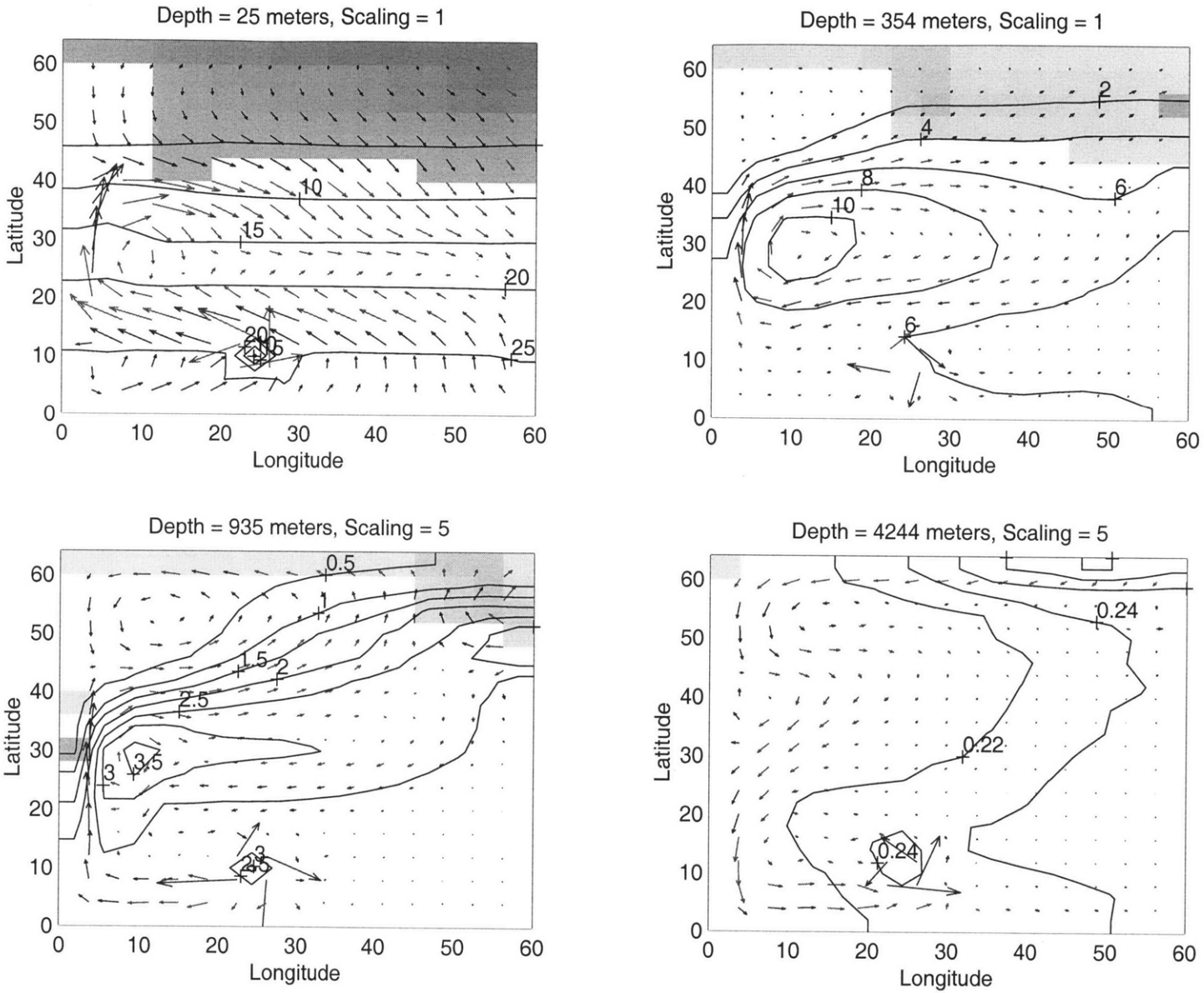

Figure 12: Velocity and temperature fields for highly localized mixing of 2 months/year, at the midpoint of the 2 months of mixing. Only horizontal cross sections are provided for comparison with the boundary mixing case. Solid contours indicate temperature. Arrows indicate fluid velocities. Convection is shown by shading, with the degree of shading indicating the time rate of change of temperature due to convection.